J Math Chem (2015) 53:1010–1053
DOI 10.1007/s10910-014-0467-1

ORIGINAL PAPER

Combinatorial approach to group hierarchy for stereoskeletons of ligancy 4

Shinsaku Fujita

Received: 15 September 2014 / Accepted: 19 December 2014 / Published online: 31 December 2014

Abstract Fujita's proligand method developed originally for combinatorial enumeration under point groups (Fujita in Theor Chem Acc 113:73–79, 2005) is extended to meet the group hierarchy, which stems from the stereoisogram approach for integrating geometric aspects and stereoisomerism in stereochemistry (Fujita in J Org Chem 69:3158–3165, 2004). Thereby, it becomes applicable to enumeration under respective levels of the group hierarchy. Combinatorial enumerations are conducted to count inequivalent pairs of (self-)enantiomers under a point group, inequivalent quadruplets of *RS*-stereoisomers under an *RS*-stereoisomeric group, inequivalent sets of stereoisomers under a stereoisomeric group, and inequivalent sets of isoskeletomers under an isoskeletal group. In these enumerations, stereoskeletons of ligancy 4 are used as examples, i.e., a tetrahedral skeleton, an allene skeleton, an ethylene skeleton, an oxirane skeleton, a square planar skeleton, and a square pyramidal skeleton. Two kinds of compositions are used for the purpose of representing molecular formulas in an abstract fashion, that is to say, the compositions for differentiating proligands having opposite chirality senses and the compositions for equalizing proligands having opposite chirality senses. Thereby, the classifications of isomers are accomplished in a systematic fashion.

Keywords Proligand method · Ligancy 4 · Stereoskeleton · Group hierarchy · Stereoisomer · Stereoisogram · Enumeration

S. Fujita (✉)
Shonan Institute of Chemoinformatics and Mathematical Chemistry,
Kaneko 479-7 Ooimachi, Ashigara-Kami-Gun, Kanagawa-Ken 258-0019, Japan
e-mail: shinsaku_fujita@nifty.com

1 Introduction

Pólya's theorem [1,2] has long been a standard method for combinatorial enumeration, as found in many reviews [3,4] and books [5–8]. It has been widely applied to chemistry as summarized in reviews [9–12] and books [13–15], where chemical compounds are regarded as two-dimensional (2D) structures (or graphs). As found in Pólya's original paper [1,2], such 2D structures (or graphs) are considered to belong to permutation groups, where ligands (substituents) are regarded as 2D structures (or graphs).

To enumerate chemical compounds as three-dimensional (3D) structures, the proligand method [16–18] has been developed by us, where Pólya's cycle indices (CIs) were extended to cycle indices with chirality fittingness (CI-CFs). The crux of the proligand method is the concept of sphericities for classifying cycles to homospheric, enantiospheric, and hemispheric ones, as discussed in a review [19]. Thereby, each classified cycle is characterized by chirality fittingness (CF) for accommodating proligands, which are presumed to be abstract entities for representing concrete ligands (substituents) having 3D structures.

Fujita's proligand method and related methods have been applied to enumerate alkanes and mono-substituted alkanes [20–22], cubane derivatives [23–25], and other molecular entities, as summarized in reviews [19,26] and books [27,28]. The concept of sphericities for cycles is correlated to cyclic subgroups of point groups [16], so that such 3D structures are presumed to belong to point groups in Fujita's proligand method, where ligands having 3D structures are regarded as proligands with chirality/achirality.

We have recently developed the stereoisogram approach [29–32], where the permutation groups are restricted to *RS*-permutation groups and integrated with point groups, so as to generate *RS*-stereoisomeric groups. Stereoisograms have been developed as diagrammatic representations of each *RS*-stereoisomeric group and its subgroups. By starting from *RS*-stereoisomeric groups, we are able to construct stereoisomeric groups and isoskeletal groups as groups of higher hierarchy [33–36]. For the purpose of comprehending the relationships between these higher-level groups, more quantitative discussions are desirable, where Fujita's proligand method under point groups should be extended to be applicable to these higher-level groups.

The present article is devoted to an extension of Fujita's proligand method to cover such higher-level groups as *RS*-stereoisomeric groups, stereoisomeric groups, and isoskeletal groups, where various stereoskeletons of ligancy 4 are examined as examples in an integrated manner. Thereby, the concept of sphericities of cycles, which is based originally on point groups, can be extended to comprehend the higher-level groups.

2 Theoretical formulations

2.1 Stereoskeletons of ligancy 4

Representative stereoskeletons of ligancy 4 are shown in Fig. 1. The four positions of each stereoskeleton construct an equivalence class (orbit), which is governed by a coset representation (CR) of the point group of the stereoskeleton. The four positions

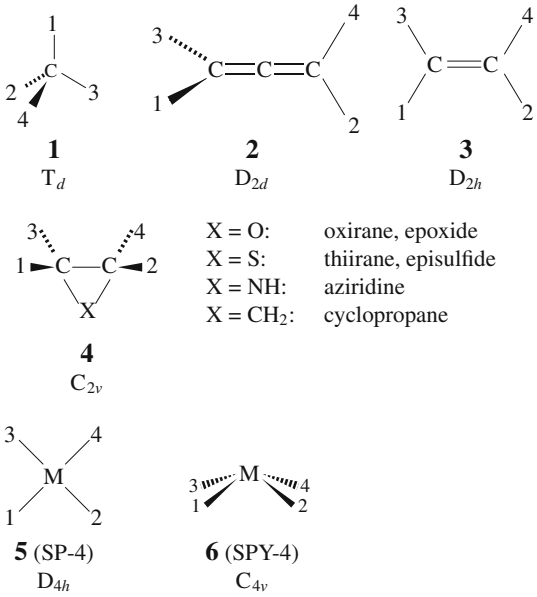

Fig. 1 Stereoskeletons of ligancy 4. The point-group symmetry of each stereoskeleton is shown by using the Schönflies notation. The symbol M represents a central metal

of a tetrahedral skeleton **1** construct an orbit governed by the CR $\mathbf{T}_d(/\mathbf{C}_{3v})$, where the resulting set of products of cycles is isomorphic to the symmetric group of degree 4 ($\mathbf{S}^{[4]}$) [27,37]. In a similar way, the other stereoskeletons collected in Fig. 1 are characterized by the following coset representations (CRs): the CR $\mathbf{D}_{2d}(/\mathbf{C}_s)$ for an allene skeleton **2** [38], the CR $\mathbf{D}_{2h}(/\mathbf{C}''_s)$ for an ethylene skeleton **3** [39], the CR $\mathbf{C}_{2v}(/\mathbf{C}_1)$ for an oxirane skeleton **4** [40], the CR $\mathbf{D}_{4h}(/\mathbf{C}''_{2v})$ for a square planar skeleton **5** (*SP*-4) [41], and the CR $\mathbf{C}_{4v}(/\mathbf{C}'_s)$ for a square pyramidal skeleton **6** (*SPY*-4). These CRs are isomorphic to the subgroups of the symmetric group of degree 4 ($\mathbf{S}^{[4]}$).

It should be noted that these CRs of the point groups are different in the action onto chiral ligands from the subgroups of the symmetric group of degree 4 ($\mathbf{S}^{[4]}$) [42]. Table 1 lists the CR $\mathbf{T}_d(/\mathbf{C}_{3v})$ of the point group $\mathbf{T}_d$ in the upper-left and lower-left parts (designated gray letters **A** and **B**) as well as the symmetric group of degree 4 ($\mathbf{S}^{[4]}$) [42] in the upper-left and upper-right parts (designated by gray letters **A** and **C**).

Although each product of cycles in the lower-left part (designated by **B**) has the same form as that of the upper-right part (designated by **C**), the former is attached by an overbar whereas the latter is not attached. This means that the former (e.g., $\overline{(1)(2\ 4)(3)}$ for $\sigma_{d(1)}$) is different in the action onto chiral ligands from the latter (e.g., $(1)(2\ 4)(3)$: cf. $\widetilde{\sigma}_{d(1)} \in \mathbf{T}_{d\widetilde{\sigma}\widehat{I}}$ described later).

2.2 *RS*-stereoisomeric groups

By starting from the point group $\mathbf{T}_d$, the stereoisogram approach derives the corresponding *RS*-stereoisomeric group denoted by the symbol $\mathbf{T}_{d\widetilde{\sigma}\widehat{I}}$ as follows [29,33]:

Table 1 Operations of $\mathbf{T}_{d\widetilde{\sigma}\widehat{I}}$ and coset representation of $\mathbf{T}_{d\widetilde{\sigma}\widehat{I}}(/\mathbf{C}_{3v\widetilde{\sigma}\widehat{I}})$ versus operations of $\mathbf{O}_h$ and coset representation of $\mathbf{O}_h(/\mathbf{D}_{3d})$ in comparison with $\mathbf{S}^{[4]}_{\sigma\widehat{I}}$

operation $g \in \mathbf{O}_h$	operation $g \in \mathbf{T}_{d\widetilde{\sigma}\widehat{I}}$	$\mathbf{O}_h(/\mathbf{D}_{3d})$ or $\mathbf{T}_{d\widetilde{\sigma}\widehat{I}}(/\mathbf{C}_{3v\widetilde{\sigma}\widehat{I}})$ or $g \in \mathbf{S}^{[4]}_{\sigma\widehat{I}}$ (product of cycles, product of SIs)		operation $g \in \mathbf{O}_h$	operation $g \in \mathbf{T}_{d\widetilde{\sigma}\widehat{I}}$	$\mathbf{O}_h(/\mathbf{D}_{3d})$ or $\mathbf{T}_{d\widetilde{\sigma}\widehat{I}}(/\mathbf{C}_{3v\widetilde{\sigma}\widehat{I}})$ or $g \in \mathbf{S}^{[4]}_{\sigma\widehat{I}}$ (product of cycles, product of SIs)	
I	I	$(1)(2)(3)(4)$	b_1^4	$C'_{2(6)}$	$\widetilde{\sigma}_{d(1)}$	$(1)(2\,4)(3)$	$b_1^2b_2$
$C_{2(1)}$	$C_{2(1)}$	$(1\,2)(3\,4)$	b_2^2	$C'_{2(1)}$	$\widetilde{\sigma}_{d(6)}$	$(1\,3)(2)(4)$	$b_1^2b_2$
$C_{2(2)}$	$C_{2(2)}$	$(1\,4)(2\,3)$	b_2^2	$C'_{2(4)}$	$\widetilde{\sigma}_{d(5)}$	$(1\,4)(2)(3)$	$b_1^2b_2$
$C_{2(3)}$	$C_{2(3)}$	$(1\,3)(2\,4)$	b_2^2	$C'_{2(2)}$	$\widetilde{\sigma}_{d(2)}$	$(1)(2)(3\,4)$	$b_1^2b_2$
$C_{3(1)}$	$C_{3(1)}$	$(1)(2\,3\,4)$	b_1b_3	$C'_{2(5)}$	$\widetilde{\sigma}_{d(3)}$	$(1)(2\,3)(4)$	$b_1^2b_2$
$C_{3(3)}$	$C_{3(3)}$	$(1\,3\,4)(3)$	b_1b_3	$C'_{2(3)}$	$\widetilde{\sigma}_{d(4)}$	$(1\,2)(3)(4)$	$b_1^2b_2$
$C_{3(2)}$	$C_{3(2)}$	$(1\,4\,3)(2)$	b_1b_3	$C^3_{4(3)}$	$\widetilde{S}_{4(3)}$	$(1\,2\,3\,4)$	b_4
$C_{3(4)}$	$C_{3(4)}$	$(1\,3\,2)(4)$	b_1b_3	$C_{4(3)}$	$\widetilde{S}^3_{4(3)}$	$(1\,4\,3\,2)$	b_4
$C^2_{3(1)}$	$C^2_{3(1)}$	$(1)(2\,4\,3)$	b_1b_3	$C^3_{4(1)}$	$\widetilde{S}^3_{4(1)}$	$(1\,4\,2\,3)$	b_4
$C^2_{3(4)}$	$C^2_{3(4)}$	$(1\,2\,3)(4)$	b_1b_3	$C_{4(1)}$	$\widetilde{S}_{4(1)}$	$(1\,3\,2\,4)$	b_4
$C^2_{3(3)}$	$C^2_{3(3)}$	$(1\,4\,2)(3)$	b_1b_3	$C_{4(2)}$	$\widetilde{S}^3_{4(2)}$	$(1\,2\,4\,3)$	b_4
$C^2_{3(2)}$	$C^2_{3(2)}$	$(1\,3\,4)(2)$	b_1b_3	$C^3_{4(2)}$	$\widetilde{S}_{4(2)}$	$(1\,3\,4\,2)$	b_4
$\sigma_{d(1)}$	$\sigma_{d(1)}$	$\overline{(1)(2\,4)(3)}$	$a_1^2c_2$	i	$\widehat{I}$	$\overline{(1)(2)(3)(4)}$	a_1^4
$\sigma_{d(6)}$	$\sigma_{d(6)}$	$\overline{(1\,3)(2)(4)}$	$a_1^2c_2$	$\sigma_{h(3)}$	$\widehat{C}_{2(1)}$	$\overline{(1\,2)(3\,4)}$	c_2^2
$\sigma_{d(2)}$	$\sigma_{d(2)}$	$\overline{(1)(2)(3\,4)}$	$a_1^2c_2$	$\sigma_{h(2)}$	$\widehat{C}_{2(2)}$	$\overline{(1\,4)(2\,3)}$	c_2^2
$\sigma_{d(4)}$	$\sigma_{d(4)}$	$\overline{(1\,2)(3)(4)}$	$a_1^2c_2$	$\sigma_{h(1)}$	$\widehat{C}_{2(3)}$	$\overline{(1\,3)(2\,4)}$	c_2^2
$\sigma_{d(3)}$	$\sigma_{d(3)}$	$\overline{(1)(2\,3)(4)}$	$a_1^2c_2$	$S^5_{6(1)}$	$\widehat{C}_{3(1)}$	$\overline{(1)(2\,3\,4)}$	a_1a_3
$\sigma_{d(5)}$	$\sigma_{d(5)}$	$\overline{(1\,4)(2)(3)}$	$a_1^2c_2$	$S^5_{6(3)}$	$\widehat{C}_{3(3)}$	$\overline{(1\,4\,2)(3)}$	a_1c_3
$S_{4(3)}$	$S_{4(3)}$	$\overline{(1\,2\,3\,4)}$	c_4	$S^5_{6(2)}$	$\widehat{C}_{3(2)}$	$\overline{(1\,4\,3)(2)}$	a_1a_3
$S^3_{4(3)}$	$S^3_{4(3)}$	$\overline{(1\,4\,3\,2)}$	c_4	$S^5_{6(4)}$	$\widehat{C}_{3(4)}$	$\overline{(1\,2\,3)(4)}$	a_1a_3
$S_{4(1)}$	$S_{4(1)}$	$\overline{(1\,4\,2\,3)}$	c_4	$S_{6(1)}$	$\widehat{C}^2_{3(1)}$	$\overline{(1)(2\,4\,3)}$	a_1a_3
$S^3_{4(1)}$	$S^3_{4(1)}$	$\overline{(1\,3\,2\,4)}$	c_4	$S_{6(4)}$	$\widehat{C}_{3(4)^2}$	$\overline{(1\,3\,2)(4)}$	a_1a_3
$S^3_{4(2)}$	$S^3_{4(2)}$	$\overline{(1\,2\,4\,3)}$	c_4	$S_{6(3)}$	$\widehat{C}^2_{3(3)}$	$\overline{(1\,2\,4)(3)}$	a_1a_3
$S_{4(2)}$	$S_{4(2)}$	$\overline{(1\,3\,4\,2)}$	c_4	$S_{6(2)}$	$\widehat{C}^2_{3(2)}$	$\overline{(1\,3\,4)(2)}$	a_1a_3

$$\begin{aligned}\mathbf{T}_{d\widetilde{\sigma}\widehat{I}} &= \mathbf{T}_d + \widetilde{\sigma}\mathbf{T}_d \\ &= \mathbf{T} + \sigma\mathbf{T} + \widetilde{\sigma}\mathbf{T} + \widehat{I}\mathbf{T},\end{aligned} \tag{1}$$

where $\widetilde{\sigma}$ is selected from the lower-left part (**B**) by omitting an overbar (e.g., $(1)(2\,4)(3)$ for $\widetilde{\sigma}_{d(1)}$ which is derived from $\overline{(1)(2\,4)(3)}$ for $\sigma_{d(1)}$), and $\widehat{I}$ ($\sim\ \overline{(1)(2)(3)(4)}$) is calculated to be $\widehat{I} = \widetilde{\sigma}_{d(1)}\sigma_{d(1)}$. The cosets of Eq. 1 correspond to the four parts of Table 1: $\mathbf{T}$ to the upper-left part (**A**), $\sigma\mathbf{T}$ to the lower-left part (**B**), $\widetilde{\sigma}\mathbf{T}$ to the upper-right part (**C**), and $\widehat{I}\mathbf{T}$ to the lower-right part (**D**).

As shown in Table 1, the *RS*-stereoisomeric group $\mathbf{T}_{d\widetilde{\sigma}\widehat{I}}$ is isomorphic to the point group $\mathbf{O}_h$. The point group $\mathbf{O}_h$ has 33 subgroups up to conjugacy, which have been

discussed in detail in terms of a non-redundant set of subgroups (SSG) [43]. Because of the isomorphism between $\mathbf{T}_{d\widetilde{\sigma}\widehat{I}}$ and $\mathbf{O}_h$, the group $\mathbf{T}_{d\widetilde{\sigma}\widehat{I}}$ has 33 subgroups up to conjugacy, which are summarized to give a non-redundant set of subgroups (SSG) for $\mathbf{T}_{d\widetilde{\sigma}\widehat{I}}$ as follows [44]:

$$\begin{aligned}\mathrm{SSG}_{\mathbf{T}_{d\widetilde{\sigma}\widehat{I}}} = \Big\{ & \overset{1}{\mathbf{C}}_1, \overset{2}{\mathbf{C}}_2, \overset{3}{\mathbf{C}}_{\widetilde{\sigma}}, \overset{4}{\mathbf{C}}_{\widehat{\sigma}}, \overset{5}{\mathbf{C}}_s, \overset{6}{\mathbf{C}}_{\widehat{I}}, \overset{7}{\mathbf{C}}_3, \overset{8}{\mathbf{S}}_{\widetilde{4}}, \overset{9}{\mathbf{S}}_4, \overset{10}{\mathbf{D}}_2, \\ & \overset{11}{\mathbf{C}}_{2\widetilde{\sigma}}, \overset{12}{\mathbf{C}}_{2\widehat{\sigma}}, \overset{13}{\mathbf{C}}_{2v}, \overset{14}{\mathbf{C}}_{s\widetilde{\sigma}\widehat{\sigma}}, \overset{15}{\mathbf{C}}_{2\widehat{I}}, \overset{16}{\mathbf{C}}_{s\widetilde{\sigma}\widehat{I}}, \overset{17}{\mathbf{C}}_{3\widetilde{\sigma}}, \overset{18}{\mathbf{C}}_{3v}, \overset{19}{\mathbf{C}}_{3\widehat{I}}, \overset{20}{\mathbf{D}}_{2\widetilde{\sigma}}, \\ & \overset{21}{\mathbf{S}}_{\widetilde{4}\widehat{\sigma}}, \overset{22}{\mathbf{S}}_{\widetilde{4}\widehat{I}}, \overset{23}{\mathbf{D}}_{2d}, \overset{24}{\mathbf{S}}_{4\widetilde{\sigma}\widehat{\sigma}}, \overset{25}{\mathbf{D}}_{2\widehat{I}}, \overset{26}{\mathbf{C}}_{2v\widetilde{\sigma}\widehat{I}}, \overset{27}{\mathbf{T}}, \overset{28}{\mathbf{C}}_{3v\widetilde{\sigma}\widehat{I}}, \overset{29}{\mathbf{D}}_{2d\widetilde{\sigma}\widehat{I}}, \overset{30}{\mathbf{T}}_{\widetilde{\sigma}}, \\ & \overset{31}{\mathbf{T}}_{\widehat{I}}, \overset{32}{\mathbf{T}}_d, \overset{33}{\mathbf{T}}_{d\widetilde{\sigma}\widehat{I}} \Big\}, \end{aligned} \tag{2}$$

where the subgroups are aligned in the ascending order of their orders. For the convenience of cross reference, sequential numbers from 1 to 33 are attached to the respective subgroups. The four positions of the tetrahedral skeleton **1** are governed by the CR $\mathbf{T}_{d\widetilde{\sigma}\widehat{I}}(/\mathbf{C}_{3v\widetilde{\sigma}\widehat{I}})$ under the *RS*-stereoisomeric group $\mathbf{T}_{d\widetilde{\sigma}\widehat{I}}$.

It should be noted that the *RS*-stereoisomeric group $\mathbf{T}_{d\widetilde{\sigma}\widehat{I}}$ formulated as above is effective to treat stereoskeletons other than those of ligancy 4. For example, the CR $\mathbf{T}_d(/\mathbf{C}_s)$ for characterizing twelve hydrogens on the methylene groups of an adamantane skeleton [37] can be treated by $\mathbf{T}_{d\widetilde{\sigma}\widehat{I}}$, where the CR $\mathbf{T}_{d\widetilde{\sigma}\widehat{I}}(/\mathbf{C}_{s\widetilde{\sigma}\widehat{I}})$ is taken into consideration.

2.3 Reflective symmetric groups

If we restrict our discussions to stereoskeletons of ligancy 4, the *RS*-stereoisomeric group $\mathbf{T}_{d\widetilde{\sigma}\widehat{I}}$ (strictly speaking, the CR $\mathbf{T}_{d\widetilde{\sigma}\widehat{I}}(/\mathbf{C}_{3v\widetilde{\sigma}\widehat{I}})$) can be alternatively constructed by starting from the symmetric group of degree 4 ($\mathbf{S}^{[4]}$). Note that the latter group is designated by the symbol $\mathbf{S}^{[4]}$ with a superscript to avoid confusion with the point group $\mathbf{S}_4$ of order 4 (cf. the No. 9 subgroup of Eq. 2).

Let us consider a direct product $\mathbf{S}^{[4]} \times \{I, \sigma\}$, where the symbol σ is a product of cycles for a reflection (e.g., $\sigma = \overline{(1)(2\,4)(3)} \sim \sigma_{d(1)}$). The direct product can be interpreted to be a group denoted by the symbol $\mathbf{S}^{[4]}_{\sigma\widehat{I}}$:

$$\begin{aligned}\mathbf{S}^{[4]}_{\sigma\widehat{I}} &= \mathbf{S}^{[4]} + \sigma\mathbf{S}^{[4]} \\ &= \mathbf{S}^{[4]}_{10} + \sigma\mathbf{S}^{[4]}_{10} + \widetilde{\sigma}\mathbf{S}^{[4]}_{10} + \widehat{I}\mathbf{S}^{[4]}_{10}, \end{aligned} \tag{3}$$

which is here called *a reflective symmetric group*. The reflective symmetric group $\mathbf{S}^{[4]}_{\sigma\widehat{I}}$ (Eq. 3) is derived in a similar way to Eq. 1, where we use the following coset decomposition:

$$\mathbf{S}^{[4]} = \mathbf{S}^{[4]}_{10} + \widetilde{\sigma}\mathbf{S}^{[4]}_{10}, \tag{4}$$

because $\mathbf{S}^{[4]}$ is isomorphic to $\mathbf{T}_{\tilde{\sigma}}$ ($\{\mathbf{A}, \mathbf{C}\}$) and $\mathbf{S}^{[4]}_{10}$ (= $\mathbf{A}^{[4]}$: the alternating group of degree 4) is isomorphic to $\mathbf{T}$ ($\{\mathbf{A}\}$). The reflective symmetric group $\mathbf{S}^{[4]}_{\sigma\widehat{I}}$ (Eq. 3) is isomorphic to the *RS*-stereoisomeric group $\mathbf{T}_{d\tilde{\sigma}\widehat{I}}$ (Eq. 1). These two groups can be equalized if we restrict our discussions to stereoskeletons of ligancy 4.

Because of the isomorphism between the reflective symmetric group $\mathbf{S}^{[4]}_{\sigma\widehat{I}}$ and the *RS*-stereoisomeric group $\mathbf{T}_{d\tilde{\sigma}\widehat{I}}$, the non-redundant set of subgroups (SSG) for $\mathbf{S}^{[4]}_{\sigma\widehat{I}}$ (Eq. 3) is obtained as follows:

$$\begin{aligned}\mathrm{SSG}_{\mathbf{S}^{[4]}_{\sigma\widehat{I}}} = \Big\{ & \overset{1}{\mathbf{S}^{[4]}_{1}}, \overset{2}{\mathbf{S}^{[4]}_{2}}, \overset{3}{\mathbf{S}^{[4]}_{3}}, \overset{4}{\mathbf{S}^{[4]}_{1\widehat{\sigma}}}, \overset{5}{\mathbf{S}^{[4]}_{1\sigma}}, \overset{6}{\mathbf{S}^{[4]}_{1\widehat{I}}}, \overset{7}{\mathbf{S}^{[4]}_{4}}, \overset{8}{\mathbf{S}^{[4]}_{5}}, \overset{9}{\mathbf{S}^{[4]}_{2\sigma'}}, \overset{10}{\mathbf{S}^{[4]}_{6}}, \\ & \overset{11}{\mathbf{S}^{[4]}_{7}}, \overset{12}{\mathbf{S}^{[4]}_{2\widehat{\sigma}}}, \overset{13}{\mathbf{S}^{[4]}_{2\sigma}}, \overset{14}{\mathbf{S}^{[4]}_{3\sigma\widehat{\sigma}}}, \overset{15}{\mathbf{S}^{[4]}_{2\widehat{I}}}, \overset{16}{\mathbf{S}^{[4]}_{3\sigma\widehat{I}}}, \overset{17}{\mathbf{S}^{[4]}_{8}}, \overset{18}{\mathbf{S}^{[4]}_{4\sigma}}, \overset{19}{\mathbf{S}^{[4]}_{4\widehat{I}}}, \overset{20}{\mathbf{S}^{[4]}_{9}}, \\ & \overset{21}{\mathbf{S}^{[4]}_{5\sigma\widehat{\sigma}}}, \overset{22}{\mathbf{S}^{[4]}_{5\sigma'\widehat{I}}}, \overset{23}{\mathbf{S}^{[4]}_{6\sigma}}, \overset{24}{\mathbf{S}^{[4]}_{7\sigma'\widehat{\sigma}}}, \overset{25}{\mathbf{S}^{[4]}_{6\widehat{I}}}, \overset{26}{\mathbf{S}^{[4]}_{7\sigma\widehat{I}}}, \overset{28}{\mathbf{S}^{[4]}_{8\sigma\widehat{I}}}, \overset{27}{\mathbf{S}^{[4]}_{10}}, \overset{29}{\mathbf{S}^{[4]}_{9\sigma\widehat{I}}}, \overset{30}{\mathbf{S}^{[4]}}, \\ & \overset{31}{\mathbf{S}^{[4]}_{10\widehat{I}}}, \overset{32}{\mathbf{S}^{[4]}_{10\sigma}}, \overset{33}{\mathbf{S}^{[4]}_{\sigma\widehat{I}}} \Big\}, \end{aligned} \tag{5}$$

where the symbol $\mathbf{S}^{[4]}_{i}$ ($i = 1$–11; $\mathbf{S}^{[4]}_{1} = \{I\}$ and $\mathbf{S}^{[4]}_{11} = \mathbf{S}^{[4]}$) constructs a non-redundant set of subgroups for $\mathbf{S}^{[4]}$. The subscript σ or σ' indicates the membership of products of cycles selected from the **B** part of Table 1. The subscript $\widehat{I}$ or $\widehat{\sigma}$ indicates the membership of products of cycles selected from the **D** part of Table 1.

Just as the subgroups of the *RS*-stereoisomeric group $\mathbf{T}_{d\tilde{\sigma}\widehat{I}}$ are classified to five types [44], the subgroups of the reflective symmetric group $\mathbf{S}^{[4]}_{\sigma\widehat{I}}$ are classified to five types, which correspond to stereoisograms of five types (type I–V).

The subgroup $\mathbf{S}^{[4]}_{10}$ ($\cong \mathbf{T}$) and its subgroups listed as follows correspond to type-III stereoisograms:

$$\mathbf{S}^{[4]}_{1} \cong \mathbf{C}_1 \overset{1}{=} \{I\} \tag{6}$$

$$\mathbf{S}^{[4]}_{2} \cong \mathbf{C}_2 \overset{2}{=} \{I, C_{2(3)}\} \tag{7}$$

$$\mathbf{S}^{[4]}_{4} \cong \mathbf{C}_3 \overset{7}{=} \{I, C_{3(1)}, C^2_{3(1)}\} \tag{8}$$

$$\mathbf{S}^{[4]}_{6} \cong \mathbf{D}_2 \overset{10}{=} \{I, C_{2(1)}, C_{2(2)}, C_{2(3)}\} \tag{9}$$

$$\mathbf{S}^{[4]}_{10} \cong \mathbf{T} \overset{27}{=} \{\mathbf{A}\} \tag{10}$$

The concrete elements of each subgroup can be obtained by referring to Table 1. For example, the elements of $\mathbf{S}^{[4]}_{6}$ (Eq. 9) are obtained to be

$$\{(1)(2)(3)(4),\ (1\ 2)(3\ 4),\ (1\ 4)(2\ 3),\ (1\ 3)(2\ 4)\}$$

by referring to the rows corresponding to $\{I, C_{2(1)}, C_{2(2)}, C_{2(3)}\}$ in Table 1. When referring to the previous papers [34,42], note that the symbol $\mathbf{S}^{[4]}_{7}$ in the previous papers should be replaced by the present symbol $\mathbf{S}^{[4]}_{6}$ (Eq. 9).

The subgroup $\mathbf{S}^{[4]}$ ($\cong \mathbf{T}_{\widetilde{\sigma}}$) is the symmetric group of degree 4. Its subgroups listed as follows correspond to type-II stereoisograms:

$$\mathbf{S}_3^{[4]} \cong \mathbf{C}_{\widetilde{\sigma}} \overset{3}{=} \{I, \widetilde{\sigma}_{d(1)}\} \tag{11}$$

$$\mathbf{S}_5^{[4]} \cong \mathbf{S}_{\widetilde{4}} \overset{8}{=} \{I, \widetilde{S}_{4(3)}, C_{2(3)}, \widetilde{S}_{4(3)}^3\} \tag{12}$$

$$\mathbf{S}_7^{[4]} \cong \mathbf{C}_{2\widetilde{\sigma}} \overset{11}{=} \{I, C_{2(3)}, \widetilde{\sigma}_{d(1)}, \widetilde{\sigma}_{d(6)}\} \tag{13}$$

$$\mathbf{S}_8^{[4]} \cong \mathbf{C}_{3\widetilde{\sigma}} \overset{17}{=} \{I, C_{3(1)}, C_{3(1)}^2, \widetilde{\sigma}_{d(1)}, \widetilde{\sigma}_{d(2)}, \widetilde{\sigma}_{d(3)}\} \tag{14}$$

$$\mathbf{S}_9^{[4]} \cong \mathbf{D}_{2\widetilde{\sigma}} \overset{20}{=} \{I, C_{2(1)}, C_{2(2)}, C_{2(3)}, \widetilde{\sigma}_{d(1)}, \widetilde{\sigma}_{d(6)}, \widetilde{S}_{4(3)}, \widetilde{S}_{4(3)}^3\} \tag{15}$$

$$\mathbf{S}^{[4]} \cong \mathbf{T}_{\widetilde{\sigma}} \overset{30}{=} \{\mathbf{A}, \mathbf{C}\}, \tag{16}$$

where each subgroup contains products of cycles selected from the **C**-part in addition to the **A**-part of Table 1.

The subgroup $\mathbf{S}_{10\sigma}^{[4]}$ ($\cong \mathbf{T}_d$) and its subgroups listed as follows correspond to type-V stereoisograms:

$$\mathbf{S}_{1\sigma}^{[4]} \cong \mathbf{C}_s \overset{5}{=} \{I, \sigma_{d(1)}\} \tag{17}$$

$$\mathbf{S}_{2\sigma'}^{[4]} \cong \mathbf{S}_4 \overset{9}{=} \{I, S_{4(3)}, C_{2(3)}, S_{4(3)}^3\} \tag{18}$$

$$\mathbf{S}_{2\sigma}^{[4]} \cong \mathbf{C}_{2v} \overset{13}{=} \{I, C_{2(3)}, \sigma_{d(1)}, \sigma_{d(6)}\} \tag{19}$$

$$\mathbf{S}_{4\sigma}^{[4]} \cong \mathbf{C}_{3v} \overset{18}{=} \{I, C_{3(1)}, C_{3(1)}^2, \sigma_{d(1)}, \sigma_{d(2)}, \sigma_{d(3)}\} \tag{20}$$

$$\mathbf{S}_{6\sigma}^{[4]} \cong \mathbf{D}_{2d} \overset{22}{=} \{I, C_{2(1)}, C_{2(2)}, C_{2(3)}, \sigma_{d(1)}, \sigma_{d(6)}, S_{4(3)}, S_{4(3)}^3\} \tag{21}$$

$$\mathbf{S}_{10\sigma}^{[4]} \cong \mathbf{T}_d \overset{32}{=} \{\mathbf{A}, \mathbf{B}\}, \tag{22}$$

where each subgroup contains products of cycles selected from the **B**-part in addition to the **A**-part of Table 1.

The subgroup $\mathbf{S}_{10\widehat{I}}^{[4]}$ ($\cong \mathbf{T}_{\widehat{I}}$) and its subgroups listed as follows correspond to type-I stereoisograms:

$$\mathbf{S}_{1\widehat{\sigma}}^{[4]} \cong \mathbf{C}_{\widehat{\sigma}} \overset{4}{=} \{I, \widehat{C}_{2(3)}\} \tag{23}$$

$$\mathbf{S}_{1\widehat{I}}^{[4]} \cong \mathbf{C}_{\widehat{I}} \overset{6}{=} \{I, \widehat{I}\} \tag{24}$$

$$\mathbf{S}_{2\widehat{\sigma}}^{[4]} \cong \mathbf{C}_{2\widehat{\sigma}} \overset{12}{=} \{I, C_{2(3)}, \widehat{C}_{2(1)}, \widehat{C}_{2(2)}\} \tag{25}$$

$$\mathbf{S}_{2\widehat{I}}^{[4]} \cong \mathbf{C}_{2\widehat{I}} \overset{15}{=} \{I, C_{2(3)}, \widehat{C}_{2(3)}, \widehat{I}\} \tag{26}$$

$$\mathbf{S}_{4\widehat{I}}^{[4]} \cong \mathbf{C}_{3\widehat{I}} \overset{19}{=} \{I, C_{3(1)}, C_{3(1)}^2, \widehat{I}, \widehat{C}_{3(1)}, \widehat{C}_{3(1)}^2\} \tag{27}$$

$$\mathbf{S}_{6\widehat{I}}^{[4]} \cong \mathbf{D}_{2\widehat{I}} \overset{25}{=} \{I, C_{2(1)}, C_{2(2)}, C_{2(3)}, \widehat{I}, \widehat{C}_{2(1)}, \widehat{C}_{2(2)}, \widehat{C}_{2(3)}\} \tag{28}$$

$$\mathbf{S}_{10\widehat{I}}^{[4]} \cong \mathbf{T}_{\widehat{I}} \overset{31}{=} \{\mathbf{A}, \mathbf{D}\} \tag{29}$$

where each subgroup contains products of cycles selected from the **D**-part in addition to the **A**-part of Table 1.

The group $\mathbf{S}^{[4]}_{\sigma\widehat{I}}$ ($\cong \mathbf{T}_{d\widetilde{\sigma}\widehat{I}}$) and its subgroups listed as follows correspond to type-IV stereoisograms:

$$\mathbf{S}^{[4]}_{3\sigma\widehat{\sigma}} \cong \mathbf{C}_{s\widetilde{\sigma}\widehat{\sigma}} \overset{14}{=} \{I, \widetilde{\sigma}_{d(1)}, \widehat{C}_{2(3)}, \sigma_{d(6)}\} \tag{30}$$

$$\mathbf{S}^{[4]}_{3\sigma\widehat{I}} \cong \mathbf{C}_{s\widetilde{\sigma}\widehat{I}} \overset{16}{=} \{I, \widetilde{\sigma}_{d(1)}, \widehat{I}, \sigma_{d(1)}\} \tag{31}$$

$$\mathbf{S}^{[4]}_{5\sigma\widehat{\sigma}} \cong \mathbf{S}_{4\widetilde{\sigma}\widehat{\sigma}} \overset{21}{=} \{I, \widetilde{S}_{4(3)}, C_{2(3)}, \widetilde{S}^3_{4(3)}, \widehat{C}_{2(1)}, \widehat{C}_{2(2)}, \sigma_{d(1)}, \sigma_{d(6)}\} \tag{32}$$

$$\mathbf{S}^{[4]}_{5\sigma'\widehat{I}} \cong \mathbf{S}_{4\widetilde{I}\widehat{I}} \overset{22}{=} \{I, \widetilde{S}_{4(3)}, C_{2(3)}, \widetilde{S}^3_{4(3)}, \widehat{I}, \widehat{C}_{2(3)}, S_{4(3)}, S^3_{4(3)}\} \tag{33}$$

$$\mathbf{S}^{[4]}_{7\sigma'\widehat{\sigma}} \cong \mathbf{S}_{4\widetilde{\sigma}\widehat{\sigma}} \overset{24}{=} \{I, C_{2(3)}, \widetilde{\sigma}_{d(1)}, \widetilde{\sigma}_{d(6)}, \widehat{C}_{2(1)}, \widehat{C}_{2(2)}, S_{4(3)}, S^3_{4(3)}\} \tag{34}$$

$$\mathbf{S}^{[4]}_{7\sigma\widehat{I}} \cong \mathbf{C}_{2v\widetilde{\sigma}\widehat{I}} \overset{26}{=} \{I, C_{2(3)}, \widetilde{\sigma}_{d(1)}, \widetilde{\sigma}_{d(6)}, \widehat{I}, \widehat{C}_{2(3)}, \sigma_{d(1)}, \sigma_{d(6)}\} \tag{35}$$

$$\begin{aligned}\mathbf{S}^{[4]}_{8\sigma\widehat{I}} \cong \mathbf{C}_{3v\widetilde{\sigma}\widehat{I}} \overset{28}{=} \{&I, C_{3(1)}, C^2_{3(1)}, \widetilde{\sigma}_{d(1)}, \widetilde{\sigma}_{d(2)}, \widetilde{\sigma}_{d(3)}, \widehat{I}, \widehat{C}_{3(1)}, \widehat{C}^2_{3(1)},\\ &\sigma_{d(1)}, \sigma_{d(2)}, \sigma_{d(3)}\}\end{aligned} \tag{36}$$

$$\begin{aligned}\mathbf{S}^{[4]}_{9\sigma\widehat{I}} \cong \mathbf{D}_{2d\widetilde{\sigma}\widehat{I}} \overset{29}{=} \{&I, C_{2(1)}, C_{2(2)}, C_{2(3)}, \widetilde{\sigma}_{d(1)}, \widetilde{\sigma}_{d(6)}, \widetilde{S}_{4(3)}, \widetilde{S}^3_{4(3)},\\ &\widehat{I}, \widehat{C}_{2(1)}, \widehat{C}_{2(2)}, \widehat{C}_{2(3)}, \sigma_{d(1)}, \sigma_{d(6)}, S_{4(3)}, S^3_{4(3)}\}\end{aligned} \tag{37}$$

$$\mathbf{S}^{[4]}_{\sigma\widehat{I}} \cong \mathbf{T}_{d\widetilde{\sigma}\widehat{I}} \overset{33}{=} \{\mathbf{A}, \mathbf{B}, \mathbf{C}, \mathbf{D}\}. \tag{38}$$

Note that the subgroups represented by Eqs. 30–38 contain products of cycles selected from the **A**-, **B**-, **C**-, and **D**-parts of Table 1.

The tetrahedral skeleton **1** belongs to the point group $\mathbf{T}_d$, from which the *RS*-stereoisomeric group $\mathbf{T}_{d\widetilde{\sigma}\widehat{I}}$ ($\cong \mathbf{S}^{[4]}_{\sigma\widehat{I}}$) is derived. In a similar way, the allene skeleton **2** corresponds to the *RS*-stereoisomeric group $\mathbf{D}_{2d\widetilde{\sigma}\widehat{I}}$ ($\cong \mathbf{S}^{[4]}_{9\sigma\widehat{I}}$), where the point group $\mathbf{D}_{2d}$ is extended to have parts represented by $\widetilde{\sigma}$ and $\widehat{I}$. The ethylene skeleton **3** corresponds to the *RS*-stereoisomeric group $\mathbf{D}_{2\widehat{I}}$ ($\cong \mathbf{S}^{[4]}_{6\widehat{I}}$), where the point group $\mathbf{D}_{2h}$ is remain unchanged to give $\mathbf{D}_{2\widehat{I}}$. The oxirane skeleton **4** corresponds to the *RS*-stereoisomeric group $\mathbf{C}_{2v\widetilde{\sigma}\widehat{I}}$ ($\cong \mathbf{S}^{[4]}_{7\sigma\widehat{I}}$), where the point group $\mathbf{C}_{2v}$ is extended to have parts represented by $\widetilde{\sigma}$ and $\widehat{I}$. The square planar skeleton **5** (*SP*-4) corresponds to the *RS*-stereoisomeric group $\mathbf{D}_{4\widehat{I}}$ ($\cong \mathbf{D}_{2d\widetilde{\sigma}\widehat{I}} \cong \mathbf{S}^{[4]}_{9\sigma\widehat{I}}$), where the point group $\mathbf{D}_{4h}$ is remain unchanged to give $\mathbf{D}_{4\widehat{I}}$. The square pyramidal skeleton **6** (*SPY*-4) corresponds to the *RS*-stereoisomeric group $\mathbf{C}_{4v\widetilde{\sigma}\widehat{I}}$ ($\cong \mathbf{D}_{2d\widetilde{\sigma}\widehat{I}} \cong \mathbf{S}^{[4]}_{9\sigma\widehat{I}}$), where the point group $\mathbf{C}_{4v}$ is extended to have parts represented by $\widetilde{\sigma}$ and $\widehat{I}$.

If our discussions are restricted to the stereoskeletons of ligancy 4, the *RS*-stereoisomeric groups described in the preceding paragraphs can be commonly treated as subgroups of the reflective symmetric group $\mathbf{S}^{[4]}_{\sigma\widehat{I}}$. This fact indicates the importance of the CRs of *RS*-stereoisomeric groups. For example, the CR $\mathbf{T}_{d\widetilde{\sigma}\widehat{I}}(/\mathbf{C}_{3v\widetilde{\sigma}\widehat{I}})$ is identical with the reflective symmetric group $\mathbf{S}^{[4]}_{\sigma\widehat{I}}$, where the number of substitution positions is calculated to be $|\mathbf{T}_{d\widetilde{\sigma}\widehat{I}}|/|\mathbf{C}_{3v\widetilde{\sigma}\widehat{I}}| = 48/12 = 4$.

2.4 Group hierarchy

The hierarchy of groups has been discussed to comprehend stereoisomerism [34,36, 45], where such groups as concerning stereoisomerism are categorized so as to give a hierarchy represented by

> point groups (PG) $\subseteq$ *RS*-stereoisomeric groups (*RS*-SIG) $\subseteq$ stereoisomeric groups (SIG) $\subseteq$ isoskeletal groups (ISG).

This group hierarchy can be more quantitatively discussed by adopting the reflective symmetric group $\mathbf{S}^{[4]}_{\sigma\widehat{I}}$ (Eq. 3), if our discussions are restricted to the stereoskeletons of ligancy 4 (Fig. 1). The results reported in our previous reports are cited as follows after modified from the viewpoint of the reflective symmetric group $\mathbf{S}^{[4]}_{\sigma\widehat{I}}$:

1. Hierarchy for the tetrahedral skeleton **1** [33]:

$$\mathbf{S}^{[4]}_{10\sigma}(\mathbf{T}_d) \subset \mathbf{S}^{[4]}_{\sigma\widehat{I}}(\mathbf{T}_{d\widetilde{\sigma}\widehat{I}}) = \mathbf{S}^{[4]}_{\sigma\widehat{I}} = \mathbf{S}^{[4]}_{\sigma\widehat{I}}, \tag{39}$$

   where the orders of these groups are calculated to be $|\mathbf{S}^{[4]}_{10\sigma}|$ $(= |\mathbf{T}_d|) = 24$, $|\mathbf{S}^{[4]}_{\sigma\widehat{I}}|$ $(= |\mathbf{T}_{d\widetilde{\sigma}\widehat{I}}|) = 48$, $|\mathbf{S}^{[4]}_{\sigma\widehat{I}}| = 48$, and $|\mathbf{S}^{[4]}_{\sigma\widehat{I}}| = 48$.
2. Hierarchy for the allene skeleton **2** [34]:

$$\mathbf{S}^{[4]}_{6\sigma}(\mathbf{D}_{2d}) \subset \mathbf{S}^{[4]}_{9\sigma\widehat{I}}(\mathbf{D}_{2d\widetilde{\sigma}\widehat{I}}) = \mathbf{S}^{[4]}_{9\sigma\widehat{I}} \subset \mathbf{S}^{[4]}_{\sigma\widehat{I}}, \tag{40}$$

   where the orders of these groups are calculated to be $|\mathbf{S}^{[4]}_{6\sigma}|$ $(= |\mathbf{D}_{2d}|) = 8$, $|\mathbf{S}^{[4]}_{9\sigma\widehat{I}}|$ $(= |\mathbf{D}_{2d\widetilde{\sigma}\widehat{I}}|) = 16$, $|\mathbf{S}^{[4]}_{9\sigma\widehat{I}}| = 16$, and $|\mathbf{S}^{[4]}_{\sigma\widehat{I}}| = 48$.
3. Hierarchy for the ethylene skeleton **3** [35]:

$$\mathbf{S}^{[4]}_{6\widehat{I}}(\mathbf{D}_{2h}) = \mathbf{S}^{[4]}_{6\widehat{I}}(\mathbf{D}_{2\widehat{I}}) \subset \mathbf{S}^{[4]}_{9\sigma\widehat{I}} \subset \mathbf{S}^{[4]}_{\sigma\widehat{I}}, \tag{41}$$

   where the orders of these groups are calculated to be $|\mathbf{S}^{[4]}_{6\widehat{I}}|$ $(= |\mathbf{D}_{2h}|) = 8$, $|\mathbf{S}^{[4]}_{6\widehat{I}}|$ $(= |\mathbf{D}_{2\widehat{I}}|) = 8$, $|\mathbf{S}^{[4]}_{9\sigma\widehat{I}}| = 16$, and $|\mathbf{S}^{[4]}_{\sigma\widehat{I}}| = 48$.
4. Hierarchy for the oxirane skeleton **4**:

$$\mathbf{S}^{[4]}_{2\widetilde{\sigma}}(\mathbf{C}_{2v}) \subset \mathbf{S}^{[4]}_{6\widehat{I}}(\mathbf{C}_{2v\widetilde{\sigma}\widehat{I}}) \subset \mathbf{S}^{[4]}_{9\sigma\widehat{I}} \subset \mathbf{S}^{[4]}_{\sigma\widehat{I}}, \tag{42}$$

   where the orders of these groups are calculated to be $|\mathbf{S}^{[4]}_{2\widetilde{\sigma}}|$ $(= |\mathbf{C}_{2v}|) = 4$, $|\mathbf{S}^{[4]}_{6\widehat{I}}|$ $(= \mathbf{C}_{2v\widetilde{\sigma}\widehat{I}}|) = 8$, $|\mathbf{S}^{[4]}_{9\sigma\widehat{I}}| = 16$, and $|\mathbf{S}^{[4]}_{\sigma\widehat{I}}| = 48$. Note that $\mathbf{S}^{[4]}_{2\widetilde{\sigma}}$ corresponds to the point group $\mathbf{C}_{2v}$ and that $\mathbf{S}^{[4]}_{6\widehat{I}}$ corresponds to $\mathbf{C}_{2v\widetilde{\sigma}\widehat{I}}$ derived from the point group $\mathbf{C}_{2v}$. This exhibits a different behavior from Eq. 35.
5. Hierarchy for the square planar skeleton **5** [36]:

$$\mathbf{S}^{[4]}_{9\sigma\widehat{I}}(\mathbf{D}_{4h}) = \mathbf{S}^{[4]}_{9\sigma\widehat{I}}(\mathbf{D}_{4\widehat{I}}) \subset \mathbf{S}^{[4]}_{\sigma\widehat{I}} = \mathbf{S}^{[4]}_{\sigma\widehat{I}}, \tag{43}$$

where the orders of these groups are calculated to be $|\mathbf{S}^{[4]}_{9\sigma\widehat{I}}|$ $(= |\mathbf{D}_{4h}|) = 16$, $|\mathbf{S}^{[4]}_{9\sigma\widehat{I}}|$ $(= |\mathbf{D}_{4\widehat{I}}|) = 16$, $|\mathbf{S}^{[4]}_{\sigma\widehat{I}}| = 48$, and $|\mathbf{S}^{[4]}_{\sigma\widehat{I}}| = 48$.

6. Hierarchy for the square pyramidal skeleton **6**:

$$\mathbf{S}^{[4]}_{5\sigma\widehat{\sigma}}(\mathbf{C}_{4v}) \subset \mathbf{S}^{[4]}_{9\sigma\widehat{I}}(\mathbf{C}_{4v\widetilde{\sigma}\widehat{I}}) \subset \mathbf{S}^{[4]}_{\sigma\widehat{I}} = \mathbf{S}^{[4]}_{\sigma\widehat{I}}, \tag{44}$$

where the orders of these groups are calculated to be $|\mathbf{S}^{[4]}_{5\sigma\widehat{\sigma}}|$ $(= |\mathbf{C}_{4v}|) = 8$, $|\mathbf{S}^{[4]}_{9\sigma\widehat{I}}|$ $(= |\mathbf{C}_{4v\widetilde{\sigma}\widehat{I}}|) = 16$, $|\mathbf{S}^{[4]}_{\sigma\widehat{I}}| = 48$, and $|\mathbf{S}^{[4]}_{\sigma\widehat{I}}| = 48$.

When referring to the previous papers [34,35], the symbol $\mathbf{S}^{[4]}_{7}$ in the previous papers should be replaced by the present symbol $\mathbf{S}^{[4]}_{6}$ $(\mathbf{D}_2)$ for the sake of consistency of symbols. Note that the *RS*-stereoisomeric group $\mathbf{D}_{2d\widetilde{\sigma}\widehat{I}}$, $\mathbf{D}_{4\widehat{I}}$, and $\mathbf{C}_{4v\widetilde{\sigma}\widehat{I}}$, which are derived from the respective point groups, are commonly correlated to the subgroup $\mathbf{S}^{[4]}_{9\sigma\widehat{I}}$ of order 16.

2.5 Combinatorial enumerations

The concept of *sphericities of cycles* developed for the proligand method [16] can be extended to treat reflective symmetric groups such as $\mathbf{S}^{[4]}_{\sigma\widehat{I}}$, because the permutation group **P** for Lemmas 1 and 2 of [16] can be equalized to $\mathbf{S}^{[4]}_{\sigma\widehat{I}}$ (or to $\mathbf{S}^{[n]}_{\sigma\widehat{I}}$ in general). This means that the concept of *sphericity indices* is also extended to meet the present cases concerning $\mathbf{S}^{[4]}_{\sigma\widehat{I}}$ (or generally $\mathbf{S}^{[n]}_{\sigma\widehat{I}}$). Thus, the sphericity index (SI) a_d is assigned to a homospheric cycle which is an odd-cycle contained in a permutation of $\mathbf{S}^{[4]}_{\sigma\widehat{I}} - \mathbf{S}^{[4]}$, the SI c_d is assigned to an enantiospheric cycle which is an even-cycle contained in a permutation of $\mathbf{S}^{[4]}_{\sigma\widehat{I}} - \mathbf{S}^{[4]}$, and the SI b_d is assigned to a hemispheric cycle which is an odd- or even-cycle contained in a permutation of $\mathbf{S}^{[4]}$. Thereby, each permutation of $\mathbf{S}^{[4]}_{\sigma\widehat{I}}$ is characterized by a product of sphericity indices, which is collected in the 'product-of-SIs' column of Table 1.

According to the proligand method [16–18], a cycle index with chirality fittingness (CI-CF) is calculated to characterize each of the subgroups appearing in Eqs. 39–44, where the products of SIs at issue (Table 1) are added and the resulting sum is divided by the order of the subgroup.

$$\begin{aligned}\text{CI-CF}(\mathbf{S}^{[4]}_{\sigma\widehat{I}}) = \frac{1}{48}\Big(&b_1^4 + 3b_2^2 + 8b_1b_3 + 6b_1^2b_2 + 6b_4 \\ &+ 6a_1^2c_2 + 6c_4 + a_1^4 + 3c_2^2 + 8a_1a_3\Big)\end{aligned} \tag{45}$$

$$\text{CI-CF}(\mathbf{S}^{[4]}_{10\sigma}) = \frac{1}{24}\left(b_1^4 + 3b_2^2 + 8b_1b_3 + 6a_1^2c_2 + 6c_4\right) \tag{46}$$

$$\text{CI-CF}(\mathbf{S}^{[4]}_{9\sigma\widehat{I}}) = \frac{1}{16}\left(b_1^4 + 3b_2^2 + 2b_1^2b_2 + 2b_4 + 2a_1^2c_2 + 2c_4 + a_1^4 + 3c_2^2\right) \tag{47}$$

$$\text{CI-CF}(\mathbf{S}^{[4]}_{6\sigma}) = \frac{1}{8}\left(b_1^4 + 3b_2^2 + 2a_1^2c_2 + 2c_4\right) \tag{48}$$

$$\text{CI-CF}(\mathbf{S}^{[4]}_{6\widehat{I}}) = \frac{1}{8}\left(b_1^4 + 3b_2^2 + a_1^4 + 3c_2^2\right) \tag{49}$$

$$\text{CI-CF}(\mathbf{S}^{[4]}_{5\sigma\widehat{\sigma}}) = \frac{1}{8}\left(b_1^4 + b_2^2 + 2b_4 + 2a_1^2c_2 + 2c_2^2\right) \tag{50}$$

$$\text{CI-CF}(\mathbf{S}^{[4]}_{2\widehat{\sigma}}) = \frac{1}{4}\left(b_1^4 + b_2^2 + 2c_2^2\right) \tag{51}$$

To enumerate derivatives (promolecules) by starting from the stereoskeletons of ligancy 4 (Fig. 1), four substituents are selected from an inventory of proligands:

$$\mathbf{X} = \{\mathrm{A}, \mathrm{B}, \mathrm{X}, \mathrm{Y};\ \ \mathrm{p}, \mathrm{q}, \mathrm{r}, \mathrm{s};\ \ \overline{\mathrm{p}}, \overline{\mathrm{q}}, \overline{\mathrm{r}}, \overline{\mathrm{s}}\}, \tag{52}$$

where the letters A, B, X, and Y represent achiral proligands and the pairs of p/$\overline{\mathrm{p}}$, q/$\overline{\mathrm{q}}$, r/$\overline{\mathrm{r}}$, and s/$\overline{\mathrm{s}}$ represent pairs of enantiomeric proligands in isolation (when detached). According to Theorem 1 of [16], we use the following ligand-inventory functions:

$$a_d = \mathrm{A}^d + \mathrm{B}^d + \mathrm{X}^d + \mathrm{Y}^d \tag{53}$$

$$\begin{aligned} c_d = {} & \mathrm{A}^d + \mathrm{B}^d + \mathrm{X}^d + \mathrm{Y}^d \\ & + 2\mathrm{p}^{d/2}\overline{\mathrm{p}}^{d/2} + 2\mathrm{q}^{d/2}\overline{\mathrm{q}}^{d/2} + 2\mathrm{r}^{d/2}\overline{\mathrm{r}}^{d/2} + 2\mathrm{s}^{d/2}\overline{\mathrm{s}}^{d/2} \end{aligned} \tag{54}$$

$$\begin{aligned} b_d = {} & \mathrm{A}^d + \mathrm{B}^d + \mathrm{X}^d + \mathrm{Y}^d \\ & + \mathrm{p}^d + \mathrm{q}^d + \mathrm{r}^d + \mathrm{s}^d + \overline{\mathrm{p}}^d + \overline{\mathrm{q}}^d + \overline{\mathrm{r}}^d + \overline{\mathrm{s}}^d. \end{aligned} \tag{55}$$

These ligand-inventory functions are introduced into an CI-CF (Eqs. 45–51) to give a generating function, in which the coefficient of the term $\mathrm{A}^a\mathrm{B}^b\mathrm{X}^x\mathrm{Y}^y\mathrm{p}^p\overline{\mathrm{p}}^{\overline{p}}\mathrm{q}^q\overline{\mathrm{q}}^{\overline{q}}\mathrm{r}^r\overline{\mathrm{q}}^{\overline{r}}\mathrm{s}^s\overline{\mathrm{q}}^{\overline{s}}$ indicates the number of promolecules to be counted. Because the proligands A, B, etc. appear symmetrically, the term can be represented by the following partition:

$$[\theta] = [a, b, x, y;\ p, \overline{p}, q, \overline{q}, r, \overline{r}, s, \overline{s}], \tag{56}$$

where we put $a \geq b \geq x \geq y$, $p \geq \overline{p}$, $q \geq \overline{q}$, $r \geq \overline{r}$, $s \geq \overline{s}$, and $p \geq q \geq r \geq s$ without losing generality. For example, the partition $[\theta]_1 = [4, 0, 0, 0; 0, 0, 0, 0, 0, 0, 0, 0]$ corresponds to the terms A^4, B^4, and so on.

Under the action of a point group onto each stereoskeleton (Fig. 1), a pair of (self-)enantiomers is counted once, where a self-enantiomeric relationship generates an achiral promolecule. Hence, each coefficient of the term corresponding to the partition $[\theta]_i$ represents the number of inequivalent pairs under the action of the point group, as collected in the PG-column of each table. Under an *RS*-stereoisomeric group, a quadruplet of promolecules (contained in a stereoisogram) is counted once. Hence, each coefficient for $[\theta]_i$ represents the number of inequivalent quadruplets (or stereoisograms) under the action of the *RS*-stereoisomeric group, as collected in the *RS*-SIG-column of each table. Under a stereoisomeric group, a set of stereoisomers is counted once. Hence, each coefficient for $[\theta]_i$ represents the number of inequivalent sets under the action of the stereoisomeric group, as collected in the SIG-column of each table. Under an isoskeletal group, a set of isoskeletomers is counted once. Hence,

each coefficient for $[\theta]_i$ represents the number of inequivalent sets under the action of the isoskeletal group, as collected in the ISG-column of each table.

3 Enumeration results and discussions

3.1 Tetrahedral Skeleton

Because the tetrahedral skeleton **1** has the group hierarchy shown by Eq. 39, the CI-CF for $\mathbf{S}_{10\sigma}^{[4]}$ (Eq. 46) is used to calculate the numbers of pairs of enantiomers under the point group $\mathbf{T}_d$. After the introduction of the ligand-inventory functions (Eqs. 53–55) into the CI-CF (Eq. 46), the resulting equation is expanded to give a generating function. The coefficient of each term in the generating function shows the number of pairs of (self-)enantiomers to be counted. The results are collected in the PG-column of Table 2. On the other hand, the CI-CF for $\mathbf{S}_{\sigma\widehat{I}}^{[4]}$ (Eq. 45) is used to calculate the numbers of quadruplets of *RS*-stereoisomers under the *RS*-stereoisomeric group $\mathbf{T}_{d\widetilde{\sigma}\widehat{I}}$. The results are collected in the *RS*-SIG-column of Table 2. The SIG-column (for the stereoisomeric group) or the ISG-column (for the isoskeletal group) of Table 2 has equal values to those of the *RS*-SIG-column according to the group hierarchy (Eq. 39).

To survey the results of Table 2, it is convenient to focus our attention to the *RS*-SIG-column, because the corresponding stereoisograms are capable of linking geometric features (the PG-column) and stereoisomeric features (the SIG- and ISG-columns) in stereochemistry. Note that the tetrahedral cases exhibit special features that the *RS*-SIG-column has the same values as those of the SIG- and ISG-columns.

Let us first examine the $[\theta]_{11}$-row which corresponds to the composition ABXp (or ABX$\overline{\text{p}}$). Because a pair of enantiomers (ABXp and ABX$\overline{\text{p}}$) is counted once under the point group, the value 1 at the intersection between $[\theta]_{11}$-row and the PG-column corresponds to $2 \times \frac{1}{2}(\text{ABXp} + \text{ABX}\overline{\text{p}})$, which shows the presence of two pairs of enantiomers. They are depicted in the form of a stereoisogram of type III, as found in Fig. 2. The vertical directions of Fig. 2 indicate geometric features, so that there appear a pair of enantiomers **7/$\overline{\mathbf{7}}$** and another pair of enantiomers **8/$\overline{\mathbf{8}}$**.

The value 1/2 appearing at the intersection between between $[\theta]_{11}$-row and the *RS*-SIG-column corresponds to $1 \times \frac{1}{2}(\text{ABXp} + \text{ABX}\overline{\text{p}})$, which shows the presence of one quadruplet of *RS*-stereoisomers **7/$\overline{\mathbf{7}}$/8/$\overline{\mathbf{8}}$**, which appears in the type-III stereoisogram shown in Fig. 2.

These features of enumeration are common to type-III stereoisograms, as shown by the designation of (III) in the the *RS*-SIG-column.

In summary, the hierarchy for the tetrahedral skeleton **1** (Eq. 39) results in the following classification for characterizing the $[\theta]_{11}$-row of Table 2:

$$\{\langle([\mathbf{7}\,\overline{\mathbf{7}}]\,[\mathbf{8}\,\overline{\mathbf{8}}])\rangle\}, \tag{57}$$

where a pair of square brackets represents a pair of enantiomers (or an achiral promolecule), a pair of parentheses represents a quadruplet of *RS*-stereoisomers, a pair of angle brackets represents a set of stereoisomers, and a pair of braces represents a

Table 2 Numbers of isomers derived from a tetrahedral skeleton

Partition	PG $\mathbf{S}^{[4]}_{10\sigma}$ ($\mathbf{T}_d$)	*RS*-SIG $\mathbf{S}^{[4]}_{\sigma\widehat{I}}$ ($\mathbf{T}_{d\widetilde{\sigma}\widehat{I}}$)	SIG $\mathbf{S}^{[4]}_{\sigma\widehat{I}}$	ISG $\mathbf{S}^{[4]}_{\sigma\widehat{I}}$
$[\theta]_1 = [4,0,0,0;0,0,0,0,0,0,0,0,0,0]$	1	1 (IV)	1	1
$[\theta]_2 = [3,1,0,0;0,0,0,0,0,0,0,0,0,0]$	1	1 (IV)	1	1
$[\theta]_3 = [3,0,0,0;1,0,0,0,0,0,0,0,0,0]$	1/2	1/2 (II)	1/2	1/2
$[\theta]_4 = [2,2,0,0;0,0,0,0,0,0,0,0,0,0]$	1	1 (IV)	1	1
$[\theta]_5 = [2,0,0,0;2,0,0,0,0,0,0,0,0,0]$	1/2	1/2 (II)	1/2	1/2
$[\theta]_6 = [2,1,1,0;0,0,0,0,0,0,0,0,0,0]$	1	1 (IV)	1	1
$[\theta]_7 = [2,1,0,0;1,0,0,0,0,0,0,0,0,0]$	1/2	1/2 (II)	1/2	1/2
$[\theta]_8 = [2,0,0,0;1,1,0,0,0,0,0,0,0,0]$	1	1 (IV)	1	1
$[\theta]_9 = [2,0,0,0;1,0,1,0,0,0,0,0,0,0]$	1/2	1/2 (II)	1/2	1/2
$[\theta]_{10} = [1,1,1,1;0,0,0,0,0,0,0,0,0,0]$	1	1 (I)	1	1
$[\theta]_{11} = [1,1,1,0;1,0,0,0,0,0,0,0,0,0]$	1	1/2 (III)	1/2	1/2
$[\theta]_{12} = [1,1,0,0;2,0,0,0,0,0,0,0,0,0]$	1/2	1/2 (II)	1/2	1/2
$[\theta]_{13} = [1,1,0,0;1,1,0,0,0,0,0,0,0,0]$	2	1 (V)	1	1
$[\theta]_{14} = [1,1,0,0;1,0,1,0,0,0,0,0,0,0]$	1	1/2 (III)	1/2	1/2
$[\theta]_{15} = [1,0,0,0;3,0,0,0,0,0,0,0,0,0]$	1/2	1/2 (II)	1/2	1/2
$[\theta]_{16} = [1,0,0,0;2,1,0,0,0,0,0,0,0,0]$	1/2	1/2 (II)	1/2	1/2
$[\theta]_{17} = [1,0,0,0;2,0,1,0,0,0,0,0,0,0]$	1/2	1/2 (II)	1/2	1/2
$[\theta]_{18} = [1,0,0,0;1,1,1,0,0,0,0,0,0,0]$	1	1/2 (III)	1/2	1/2
$[\theta]_{19} = [1,0,0,0;1,0,1,0,1,0,0,0,0,0]$	1	1/2 (III)	1/2	1/2
$[\theta]_{20} = [0,0,0,0;4,0,0,0,0,0,0,0,0,0]$	1/2	1/2 (II)	1/2	1/2
$[\theta]_{21} = [0,0,0,0;3,1,0,0,0,0,0,0,0,0]$	1/2	1/2 (II)	1/2	1/2
$[\theta]_{22} = [0,0,0,0;3,0,1,0,0,0,0,0,0,0]$	1/2	1/2 (II)	1/2	1/2
$[\theta]_{23} = [0,0,0,0;2,2,0,0,0,0,0,0,0,0]$	1	1 (IV)	1	1
$[\theta]_{24} = [0,0,0,0;2,1,1,0,0,0,0,0,0,0]$	1/2	1/2 (II)	1/2	1/2
$[\theta]_{25} = [0,0,0,0;2,0,2,0,0,0,0,0,0,0]$	1/2	1/2 (II)	1/2	1/2
$[\theta]_{26} = [0,0,0,0;2,0,1,1,0,0,0,0,0,0]$	1/2	1/2 (II)	1/2	1/2
$[\theta]_{27} = [0,0,0,0;2,0,1,0,1,0,0,0,0,0]$	1/2	1/2 (II)	1/2	1/2
$[\theta]_{28} = [0,0,0,0;1,1,1,1,0,0,0,0,0,0]$	1	1 (I)	1	1
$[\theta]_{29} = [0,0,0,0;1,1,1,0,1,0,0,0,0,0]$	1	1/2 (III)	1/2	1/2
$[\theta]_{30} = [0,0,0,0;1,0,1,0,1,0,1,0,0,0]$	1	1/2 (III)	1/2	1/2

set of isoskeletomers. Note that each quadruplet of *RS*-stereoisomers composes such a stereoisogram as Fig. 2.

As the 2nd example, let us examine the $[\theta]_{12}$-row, which corresponds to the composition ABp^2 (or $AB\overline{p}^2$). The value 1/2 at the intersection between $[\theta]_{12}$-row and the PG-column corresponds to $1 \times \frac{1}{2}(ABp^2 + AB\overline{p}^2)$, which shows the presence of one pair of enantiomers. This pair is depicted in the form of a stereoisogram of type II, as found in Fig. 3. The type-II stereoisogram (Fig. 3) contains one pair of enantiomers **9/$\overline{\mathbf{9}}$**.

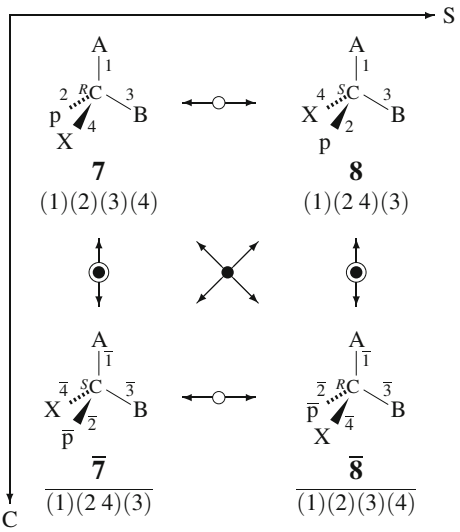

Fig. 2 Isomers with the composition ABXp or ABX$\overline{\text{p}}$ ($[\theta]_{11}$) on the basis of a tetrahedral skeleton. This diagram is a stereoisogram of type III, which contains two pairs of enantiomers

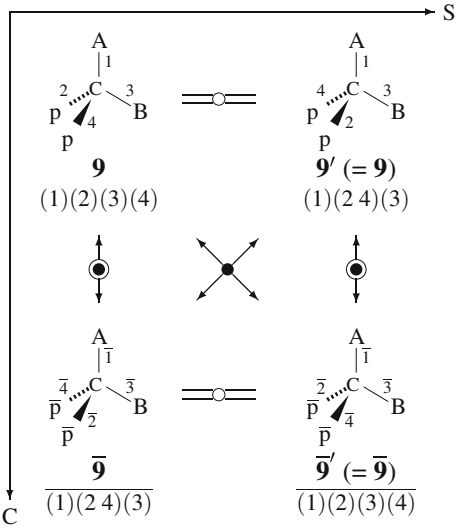

Fig. 3 Isomers with the composition ABp^2 or AB$\overline{\text{p}}^2$ ($[\theta]_{12}$) on the basis of a tetrahedral skeleton. This diagram is a stereoisogram of type II, which contains one pair of enantiomers

On the other hand, the value 1/2 at the intersection between $[\theta]_{12}$-row and the *RS*-SIG-column corresponds to $1 \times \frac{1}{2}(\text{ABp}^2 + \text{AB}\overline{\text{p}}^2)$, which shows the presence of one quadruplet of *RS*-stereoisomers, as found in Fig. 3. Because of type II, the quadruplet of the stereoisogram (Fig. 3) degenerates into one pair of enantiomers **9**/$\overline{\mathbf{9}}$

These features of enumeration exemplified by the $[\theta]_{12}$-row are common to type-II stereoisograms, as shown by each row designated by the symbol (II) at the intersection concerning the the *RS*-SIG-column.

In summary, the hierarchy for the tetrahedral skeleton **1** (Eq. 39) results in the following classification for characterizing the $[\theta]_{12}$-row of Table 2:

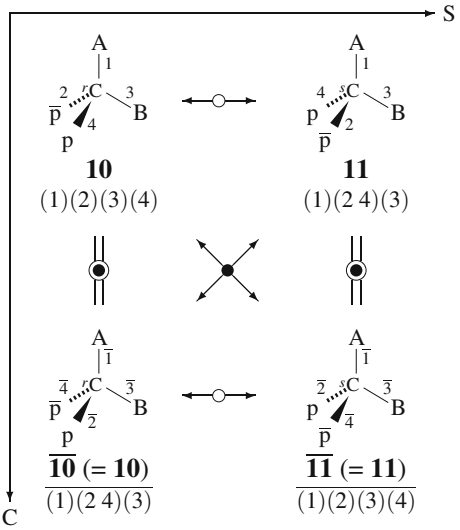

Fig. 4 Isomers with the composition ABp$\overline{\text{p}}$ ($[\theta]_{13}$) on the basis of a tetrahedral skeleton. This diagram is a stereoisogram of type V, which contains two achiral promolecules

$$\{\langle([\mathbf{9}\,\overline{\mathbf{9}}])\rangle\}, \tag{58}$$

where the quadruplet of *RS*-stereoisomers in a pair of parentheses composes such a stereoisogram as Fig. 3.

As the 3rd example, let us examine the $[\theta]_{13}$-row, which corresponds to the composition ABp$\overline{\text{p}}$. The value 2 at the intersection between $[\theta]_{13}$-row and the PG-column shows the presence of two achiral promolecules. They are depicted in the form of a type-V stereoisogram shown in Fig. 4, which contains *RS*-diastereomeric promolecules **10** and **11**.

On the other hand, the value 1 at the intersection between $[\theta]_{12}$-row and the *RS*-SIG-column shows the presence of one quadruplet of *RS*-stereoisomers (Fig. 4). Thus, a set of *RS*-diastereomeric promolecules **10/11** is regarded as one quadruplet to be counted once.

In summary, the hierarchy for the tetrahedral skeleton **1** (Eq. 39) results in the following classification for characterizing the $[\theta]_{13}$-row of Table 2:

$$\{\langle([\mathbf{10}]\,[\mathbf{11}])\rangle\}\,, \tag{59}$$

where a pair of square brackets represents an achiral promolecule as one-membered equivalence class under the point group. A quadruplet of *RS*-stereoisomers composes such a stereoisogram as Fig. 4.

3.2 Allene skeleton

Because the allene skeleton **2** has the group hierarchy shown by Eq. 40, the CI-CF for $\mathbf{S}_{6\sigma}^{[4]}$ (Eq. 48) is used to calculate the numbers of pairs of (self-)enantiomers under the point group $\mathbf{D}_{2d}$. The coefficient of each term in the corresponding generating

Table 3 Numbers of isomers derived from an allene skeleton

Partition	PG $\mathbf{S}^{[4]}_{6\sigma}$ ($\mathbf{D}_{2d}$)	*RS*-SIG $\mathbf{S}^{[4]}_{9\sigma\widehat{I}}$ ($\mathbf{D}_{2d\tilde{\sigma}\widehat{I}}$)	SIG $\mathbf{S}^{[4]}_{9\sigma\widehat{I}}$	ISG $\mathbf{S}^{[4]}_{\sigma\widehat{I}}$
$[\theta]_1 = [4,0,0,0;0,0,0,0,0,0,0,0]$	1	1	1	1
$[\theta]_2 = [3,1,0,0;0,0,0,0,0,0,0,0]$	1	1	1	1
$[\theta]_3 = [3,0,0,0;1,0,0,0,0,0,0,0]$	1/2	1/2	1/2	1/2
$[\theta]_4 = [2,2,0,0;0,0,0,0,0,0,0,0]$	2	2	2	1
$[\theta]_5 = [2,0,0,0;2,0,0,0,0,0,0,0]$	3/2	1	1	1/2
$[\theta]_6 = [2,1,1,0;0,0,0,0,0,0,0,0]$	2	2	2	1
$[\theta]_7 = [2,1,0,0;1,0,0,0,0,0,0,0]$	3/2	1	1	1/2
$[\theta]_8 = [2,0,0,0;1,1,0,0,0,0,0,0]$	2	2	2	1
$[\theta]_9 = [2,0,0,0;1,0,1,0,0,0,0,0]$	3/2	1	1	1/2
$[\theta]_{10} = [1,1,1,1;0,0,0,0,0,0,0,0]$	3	3	3	1
$[\theta]_{11} = [1,1,1,0;1,0,0,0,0,0,0,0]$	3	3/2	3/2	1/2
$[\theta]_{12} = [1,1,0,0;2,0,0,0,0,0,0,0]$	3/2	1	1	1/2
$[\theta]_{13} = [1,1,0,0;1,1,0,0,0,0,0,0]$	4	2	2	1
$[\theta]_{14} = [1,1,0,0;1,0,1,0,0,0,0,0]$	3	3/2	3/2	1/2
$[\theta]_{15} = [1,0,0,0;3,0,0,0,0,0,0,0]$	1/2	1/2	1/2	1/2
$[\theta]_{16} = [1,0,0,0;2,1,0,0,0,0,0,0]$	3/2	1	1	1/2
$[\theta]_{17} = [1,0,0,0;2,0,1,0,0,0,0,0]$	3/2	1	1	1/2
$[\theta]_{18} = [1,0,0,0;1,1,1,0,0,0,0,0]$	3	3/2	3/2	1/2
$[\theta]_{19} = [1,0,0,0;1,0,1,0,1,0,0,0]$	3	3/2	3/2	1/2
$[\theta]_{20} = [0,0,0,0;4,0,0,0,0,0,0,0]$	1/2	1/2	1/2	1/2
$[\theta]_{21} = [0,0,0,0;3,1,0,0,0,0,0,0]$	1/2	1/2	1/2	1/2
$[\theta]_{22} = [0,0,0,0;3,0,1,0,0,0,0,0]$	1/2	1/2	1/2	1/2
$[\theta]_{23} = [0,0,0,0;2,2,0,0,0,0,0,0]$	2	2	2	1
$[\theta]_{24} = [0,0,0,0;2,1,1,0,0,0,0,0]$	3/2	1	1	1/2
$[\theta]_{25} = [0,0,0,0;2,0,2,0,0,0,0,0]$	3/2	1	1	1/2
$[\theta]_{26} = [0,0,0,0;2,0,1,1,0,0,0,0]$	3/2	1	1	1/2
$[\theta]_{27} = [0,0,0,0;2,0,1,0,1,0,0,0]$	3/2	1	1	1/2
$[\theta]_{28} = [0,0,0,0;1,1,1,1,0,0,0,0]$	3	3	3	1
$[\theta]_{29} = [0,0,0,0;1,1,1,0,1,0,0,0]$	3	3/2	3/2	1/2
$[\theta]_{30} = [0,0,0,0;1,0,1,0,1,0,1,0]$	3	3/2	3/2	1/2

function gives the number of pairs of (self-)enantiomers to be counted, as collected in the PG-column of Table 3. On the other hand, the CI-CF for $\mathbf{S}^{[4]}_{9\sigma\widehat{I}}$ (Eq. 47) is used to calculate the numbers of quadruplets of *RS*-stereoisomers under the *RS*-stereoisomeric group $\mathbf{D}_{2d\tilde{\sigma}\widehat{I}}$. The results are collected in the *RS*-SIG-column of Table 3. The SIG-column (for the stereoisomeric group) has equal values to those of the *RS*-SIG-column according to the group hierarchy (Eq. 40). The ISG-column (for the isoskeletal group) of Table 3 is obtained by using the CI-CF for $\mathbf{S}^{[4]}_{\sigma\widehat{I}}$ (Eq. 45).

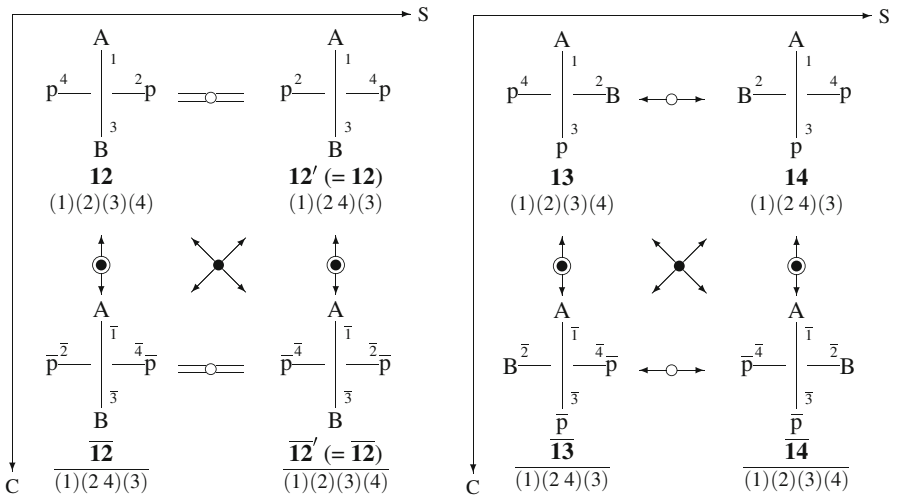

(a) type-II stereoisogram **(b)** type-III stereoisogram

Fig. 5 Stereoisograms for the composition ABp^2 (or $AB\overline{p}^2$) on the basis of the allene skeleton. **a** A type-II stereoisogram containing one pair of enantiomers. **b** A type-III stereoisogram containing two pairs of enantiomers

The enumeration results collected in the PG-column of Table 3 is equivalent to those reported previously [16], which are based on the proligand method (cf. Eq. 14 of [16]). The enumeration results collected in the *RS*-SIG-column of Table 3 is equivalent to those reported previously [46,47], which are based on the USCI method (cf. Eqs. 126 and 127 of [16]). Manual enumeration of stereoisograms for allene derivatives have been reported [34,48]. To comprehend the total features of stereoisomerism, two cases are examined from the present viewpoint as follows.

The first case is the $[\theta]_{12}$-row of Table 3, which corresponds to the composition ABp^2 (or $AB\overline{p}^2$). The value 3/2 at the intersection between $[\theta]_{12}$-row and the PG-column in Table 3 corresponds to three pairs of enantiomers because of $3 \times \frac{1}{2}(ABp^2 + AB\overline{p}^2)$. They are contained in the two stereoisograms shown in Fig. 5, where each promolecule is depicted in the form of a top projection along the C=C=C axis of the allene skeleton **2**. The type-II stereoisogram (Fig. 5a) contains one pair of enantiomers, i.e., **12**/$\overline{\mathbf{12}}$; and the type-III stereoisogram (Fig. 5b) contains two pairs of enantiomers, i.e., **13**/$\overline{\mathbf{13}}$ and **14**/$\overline{\mathbf{14}}$. Totally, there appear three pairs of enantiomers.

On the other hand, the value 1 at the intersection between $[\theta]_{12}$-row and the *RS*-SIG-column in Table 3 indicates the appearance of two quadruplets of *RS*-stereoisomers because of $2 \times \frac{1}{2}(ABp^2 + AB\overline{p}^2)$. The two quadruplets corresponds to the two stereoisograms shown in Fig. 5, so that the one quadruplet consists of *RS*-stereoisomers **12**/$\overline{\mathbf{12}}$ (degenerate) and the other quadruplet consists of *RS*-stereoisomers **13**/$\overline{\mathbf{13}}$/**14**/$\overline{\mathbf{14}}$. This result of combinatorial enumeration is consistent with the stereoisogram set denoted by $(\mathrm{II}/\mathrm{III}^2)$, which has been obtained by manual enumeration (Fig. 8 of [34]).

The hierarchy for the allene skeleton **2** (Eq. 40) indicates that the SIG-column is identical with the *RS*-SIG-column, as confirmed by Table 3. It follows that the value 1

at the intersection between the $[\theta]_{12}$-row and the SIG-column in Table 3 indicates the appearance of two inequivalent sets of stereoisomers because of $2 \times \frac{1}{2}(\mathrm{ABp}^2 + \mathrm{AB}\overline{\mathrm{p}}^2)$. In other words, each quadruplet of *RS*-stereoisomers in each stereoisogram coincides with each set of stereoisomers in the case of allene derivatives, as confirmed by Fig. 5.

Finally, the two inequivalent sets of stereoisomers (the value 1 at the SIG-column) are totally regarded as one set of isoskeletomers (the value 1/2 at the ISG-column). This result is also confirmed by Fig. 5.

In summary, the hierarchy for the allene skeleton **2** (Eq. 40) results in the following classification for characterizing the $[\theta]_{12}$-row of Table 3:

$$\{\langle([\mathbf{12}\ \overline{\mathbf{12}}])\rangle\langle([\mathbf{13}\ \overline{\mathbf{13}}]\,[\mathbf{14}\ \overline{\mathbf{14}}])\rangle\}, \tag{60}$$

where each pair of parentheses corresponds to each of the stereoisograms shown in Fig. 5.

As the 2nd case, let us examine the $[\theta]_{13}$-row of Table 3, which corresponds to the composition $\mathrm{ABp}\overline{\mathrm{p}}$. The value 4 at the intersection between $[\theta]_{13}$-row and the PG-column shows the presence of four pairs of enantiomers or achiral promolecules. They are depicted in Fig. 6a, b in the form of two stereoisograms of type V and of type III. The type-V stereoisogram (Fig. 6a) consists of two achiral promolecules **15/16**, which are *RS*-diastereomeric to each other. The type-III stereoisogram (Fig. 6b) consists of two pairs of enantiomers, i.e., **17/$\overline{\mathbf{17}}$** and **18/$\overline{\mathbf{18}}$**. Totally, there appear four pairs of (self-)enantiomeric promolecules.

On the other hand, the value 2 at the intersection between $[\theta]_{13}$-row and the *RS*-SIG-column shows the presence of two quadruplets of *RS*-stereoisomers (Fig. 6). This

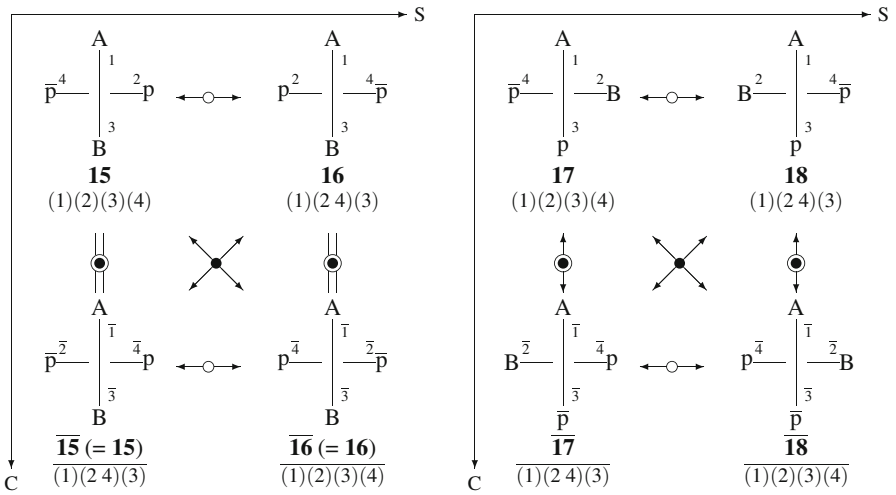

(a) type-V stereoisogram **(b)** type-III stereoisogram

Fig. 6 Stereoisograms for the composition $\mathrm{ABp}\overline{\mathrm{p}}$ on the basis of the allene skeleton. **a** A type-V stereoisogram containing two achiral promolecules. **b** A type-III stereoisogram containing two pairs of enantiomers

result of combinatorial enumeration is consistent with the stereoisogram set denoted by (V/III^2), which has been obtained by manual enumeration (Fig. 10 of [34]).

According to the hierarchy for the allene skeleton **2** (Eq. 40), the SIG-column of Table 3 is identical with the *RS*-SIG-column. Hence, each quadruplet of RS-stereoisomers (i.e., each stereoisogram) coincides with each set of stereoisomers in the case of allene derivatives, as confirmed by Fig. 6.

Finally, the two inequivalent sets of stereoisomers (the value 2 at the SIG-column) are totally regarded as one set of isoskeletomers (the value 1 at the ISG-column). This result is also confirmed by Fig. 6.

In summary, the hierarchy for the allene skeleton **2** (Eq. 40) results in the following classification for characterizing the $[\theta]_{13}$-row of Table 3:

$$\left\{\langle([\mathbf{15}]\,[\mathbf{16}])\rangle\,\langle([\mathbf{17}\,\overline{\mathbf{17}}\,]\,[\mathbf{18}\,\overline{\mathbf{18}}\,])\rangle\right\}, \tag{61}$$

where each pair of parentheses corresponds to each of the stereoisograms shown in Fig. 6.

3.3 Ethylene skeleton

The ethylene skeleton **3** has the group hierarchy shown by Eq. 41, so that the CI-CF for $\mathbf{S}^{[4]}_{6\hat{I}}$ (Eq. 49) is used to calculate the numbers of pairs of enantiomers under the point group $\mathbf{D}_{2h}$. The coefficient of each term in the obtained generating function shows the number of pairs of (self-)enantiomers to be counted, as collected in the PG-column of Table 4. The group hierarchy (Eq. 41) shows that the *RS*-stereoisomeric group $\mathbf{D}_{2\hat{I}}$ ($\cong \mathbf{S}^{[4]}_{6\hat{I}}$) is isomorphic to the point group $\mathbf{D}_{2h}$ ($\cong \mathbf{S}^{[4]}_{6\hat{I}}$). Hence, the numbers of quadruplets of *RS*-stereoisomers under the *RS*-stereoisomeric group are equal to those of pair of (self-)enantiomers, as collected in the *RS*-SIG-column of Table 4. The SIG-column (for the stereoisomeric group) has been obtained by using the CI-CF for $\mathbf{S}^{[4]}_{9\sigma\hat{I}}$ (Eq. 47) according to the group hierarchy (Eq. 41). The ISG-column (for the isoskeletal group) of Table 4 is obtained by using the CI-CF for $\mathbf{S}^{[4]}_{\sigma\hat{I}}$ (Eq. 45).

Let us examine the $[\theta]_{12}$-row of Table 4, which corresponds to the composition ABp^2 (or AB$\overline{\mathrm{p}}^2$). The value 3/2 at the intersection between $[\theta]_{12}$-row and the PG-column in Table 4 shows the presence of three pairs of enantiomers. They are contained in the three type-II stereoisograms shown in Fig. 7, i.e., **19/$\overline{\mathbf{19}}$**, **20/$\overline{\mathbf{20}}$**, and **21/$\overline{\mathbf{21}}$**. The values in *RS*-SIG-column in Table 4 are identical with the PG-column according to the hierarchy for the ethylene skeleton **3** (Eq. 41). Thus, there appear three quadruplets of *RS*-stereoisomers in accord with the three stereoisograms shown in Fig. 7.

It should be noted that the stereoisograms shown in Fig. 7 are drawn by presuming the following coset decomposition:

$$\mathbf{D}_{2\hat{I}} = \mathbf{C}_2 + \sigma\mathbf{C}_2 + \widetilde{\sigma}\mathbf{C}_2 + \widehat{I}\mathbf{C}_2, \tag{62}$$

which is derived from $\mathbf{D}_2 = \mathbf{C}_2 + \widetilde{\sigma}\mathbf{C}_2$.

The value 1 at the intersection between the $[\theta]_{12}$-row and the SIG-column in Table 4 indicates the appearance of two inequivalent sets of stereoisomers because

Table 4 Numbers of isomers derived from an ethylene skeleton

Partition	PG $\mathbf{S}_{6\widehat{I}}^{[4]}$ ($\mathbf{D}_{2h}$)	*RS*-SIG $\mathbf{S}_{6\widehat{I}}^{[4]}$ ($\mathbf{D}_{2\widehat{I}}$)	SIG $\mathbf{S}_{9\sigma\widehat{I}}^{[4]}$	ISG $\mathbf{S}_{\sigma\widehat{I}}^{[4]}$
$[\theta]_1 = [4,0,0,0;0,0,0,0,0,0,0,0]$	1	1	1	1
$[\theta]_2 = [3,1,0,0;0,0,0,0,0,0,0,0]$	1	1	1	1
$[\theta]_3 = [3,0,0,0;1,0,0,0,0,0,0,0]$	1/2	1/2	1/2	1/2
$[\theta]_4 = [2,2,0,0;0,0,0,0,0,0,0,0]$	3	3	2	1
$[\theta]_5 = [2,0,0,0;2,0,0,0,0,0,0,0]$	3/2	3/2	1	1/2
$[\theta]_6 = [2,1,1,0;0,0,0,0,0,0,0,0]$	3	3	2	1
$[\theta]_7 = [2,1,0,0;1,0,0,0,0,0,0,0]$	3/2	3/2	1	1/2
$[\theta]_8 = [2,0,0,0;1,1,0,0,0,0,0,0]$	3	3	2	1
$[\theta]_9 = [2,0,0,0;1,0,1,0,0,0,0,0]$	3/2	3/2	1	1/2
$[\theta]_{10} = [1,1,1,1;0,0,0,0,0,0,0,0]$	6	6	3	1
$[\theta]_{11} = [1,1,1,0;1,0,0,0,0,0,0,0]$	3	3	3/2	1/2
$[\theta]_{12} = [1,1,0,0;2,0,0,0,0,0,0,0]$	3/2	3/2	1	1/2
$[\theta]_{13} = [1,1,0,0;1,1,0,0,0,0,0,0]$	3	3	2	1
$[\theta]_{14} = [1,1,0,0;1,0,1,0,0,0,0,0]$	3	3	3/2	1/2
$[\theta]_{15} = [1,0,0,0;3,0,0,0,0,0,0,0]$	1/2	1/2	1/2	1/2
$[\theta]_{16} = [1,0,0,0;2,1,0,0,0,0,0,0]$	3/2	3/2	1	1/2
$[\theta]_{17} = [1,0,0,0;2,0,1,0,0,0,0,0]$	3/2	3/2	1	1/2
$[\theta]_{18} = [1,0,0,0;1,1,1,0,0,0,0,0]$	3	3	3/2	1/2
$[\theta]_{19} = [1,0,0,0;1,0,1,0,1,0,0,0]$	3	3	3/2	1/2
$[\theta]_{20} = [0,0,0,0;4,0,0,0,0,0,0,0]$	1/2	1/2	1/2	1/2
$[\theta]_{21} = [0,0,0,0;3,1,0,0,0,0,0,0]$	1/2	1/2	1/2	1/2
$[\theta]_{22} = [0,0,0,0;3,0,1,0,0,0,0,0]$	1/2	1/2	1/2	1/2
$[\theta]_{23} = [0,0,0,0;2,2,0,0,0,0,0,0]$	3	3	2	1
$[\theta]_{24} = [0,0,0,0;2,1,1,0,0,0,0,0]$	3/2	3/2	1	1/2
$[\theta]_{25} = [0,0,0,0;2,0,2,0,0,0,0,0]$	3/2	3/2	1	1/2
$[\theta]_{26} = [0,0,0,0;2,0,1,1,0,0,0,0]$	3/2	3/2	1	1/2
$[\theta]_{27} = [0,0,0,0;2,0,1,0,1,0,0,0]$	3/2	3/2	1	1/2
$[\theta]_{28} = [0,0,0,0;1,1,1,1,0,0,0,0]$	6	6	3	1
$[\theta]_{29} = [0,0,0,0;1,1,1,0,1,0,0,0]$	3	3	3/2	1/2
$[\theta]_{30} = [0,0,0,0;1,0,1,0,1,0,1,0]$	3	3	3/2	1/2

of $2 \times \frac{1}{2}(\mathrm{ABp}^2 + \mathrm{AB\overline{p}}^2)$. The *cis/trans*-isomerization of **19** (a *Z*-isomer) generates the corresponding *E*-isomer **20**, so that the stereoisogram shown by Fig. 7a is equivalent to the other stereoisogram shown by Fig. 7b under the action of the stereoisomeric group. Thereby, the quadruplets of the two stereoisograms coalesce into a single set of stereoisomers to be counted once for the SIG-column in Table 4. On the other hand, the *cis/trans*-isomerization converts **21** into itself, so that the quadruplet of Fig. 7c itself generates a single set of stereoisomers to be counted once for the SIG-column in

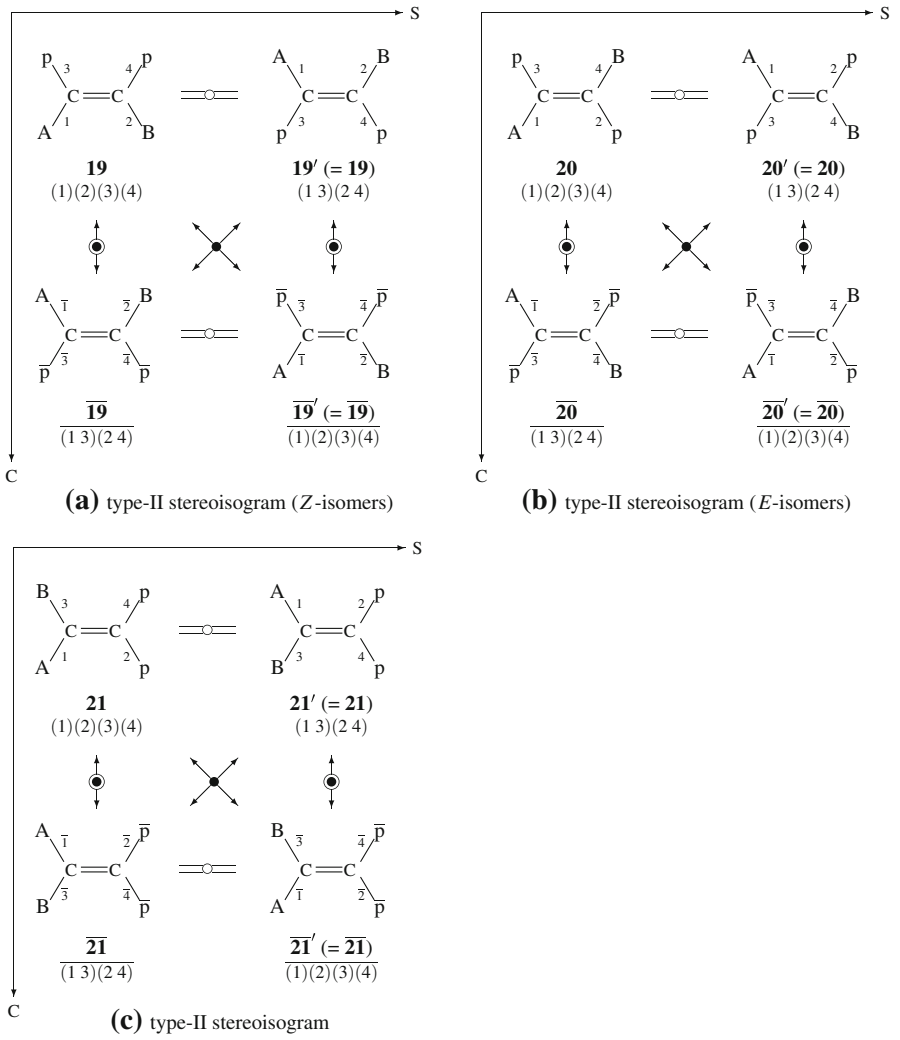

(a) type-II stereoisogram (*Z*-isomers) **(b)** type-II stereoisogram (*E*-isomers)

(c) type-II stereoisogram

Fig. 7 Stereoisograms for the composition ABp^2 (or $AB\bar{p}^2$) on the basis of the ethylene skeleton. **a** A type-II stereoisogram containing a pair of enantiomers (*Z*-isomers). **b** A type-II stereoisogram containing a pair of enantiomers (*E*-isomers). **c** A type-II stereoisogram containing a pair of enantiomers

Table 4. Totally, there appear two inequivalent sets of stereoisomers, as found at the intersection between the $[\theta]_{12}$-row and the SIG-column in Table 4.

Finally, the two inequivalent sets of stereoisomers (the value 1 at the SIG-column) are totally regarded as one set of isoskeletomers (the value 1/2 at the ISG-column). This result is also confirmed by Fig. 7, where the three stereoisograms coalesce to give a single set of isoskeletomers. This result of combinatorial enumeration is consistent with the extended stereoisogram set denoted by $(\text{II-II})^2/\text{II}^2$), which has been obtained by manual enumeration (e.g., Fig. 10 of [35]).

In summary, the hierarchy for the ethylene skeleton **3** (Eq. 41) results in the following classification for characterizing the $[\theta]_{12}$-row of Table 4:

$$\{\langle([\mathbf{19}\ \overline{\mathbf{19}}])\ ([\mathbf{20}\ \overline{\mathbf{20}}])\rangle\langle([\mathbf{21}\ \overline{\mathbf{21}}])\rangle\}, \tag{63}$$

where each pair of parentheses corresponds to each of the stereoisograms shown in Fig. 7.

Let us next examine the $[\theta]_{13}$-row of Table 4, which corresponds to the composition ABp$\overline{\text{p}}$. The value 3 at the intersection between $[\theta]_{13}$-row and the PG-column in Table 4 indicates the presence of three pairs of enantiomers, i.e., **22**/$\overline{\mathbf{22}}$, **23**/$\overline{\mathbf{23}}$, and **24**/$\overline{\mathbf{24}}$, which are respectively involved in the three type-II stereoisograms shown in Fig. 8. According to the hierarchy for the ethylene skeleton **3** (Eq. 41), the values in *RS*-SIG-column in Table 4 are identical with the PG-column. Hence, the presence of three quadruplets of *RS*-stereoisomers is concluded in accord with the three stereoisograms shown in Fig. 8.

The value 2 at the intersection between the $[\theta]_{13}$-row and the SIG-column in Table 4 indicates the appearance of two inequivalent sets of stereoisomers. The *cis/trans*-isomerization of **22** (a *Z*-isomer) generates the corresponding *E*-isomer **23**. Hence, the stereoisogram shown by Fig. 8a is equivalent to the other stereoisogram shown by Fig. 8b under the action of the stereoisomeric group. This means that the quadruplets of the two stereoisograms coalesce into a single set of stereoisomers to be counted once for the SIG-column in Table 4. On the other hand, the *cis/trans*-isomerization converts **24** into its enantiomer $\overline{\mathbf{24}}$, so that the quadruplet of Fig. 7c itself generates a single set of stereoisomers to be counted once for the SIG-column in Table 4. Totally, there appear two inequivalent sets of stereoisomers, as found at the intersection between the $[\theta]_{13}$-row and the SIG-column in Table 4.

Finally, the two inequivalent sets of stereoisomers (the value 2 at the SIG-column) are totally regarded as one set of isoskeletomers (the value 1 at the ISG-column). This result is also confirmed by Fig. 8, where the three stereoisograms coalesce to give a single set of isoskeletomers. This result of combinatorial enumeration is consistent with the extended stereoisogram set denoted by $(\text{II-II})^2/(\text{II}{=}\text{II})$, which has been obtained by manual enumeration (e.g., Fig. 14 of [35]).

In summary, the hierarchy for the ethylene skeleton **3** (Eq. 41) results in the following classification for characterizing the $[\theta]_{13}$-row of Table 4:

$$\{\langle([\mathbf{22}\ \overline{\mathbf{22}}])\ ([\mathbf{23}\ \overline{\mathbf{23}}])\rangle\langle([\mathbf{24}\ \overline{\mathbf{24}}])\rangle\}, \tag{64}$$

where each pair of parentheses corresponds to each of the stereoisograms shown in Fig. 8.

It should be noted that the enantiomeric relationship between **24** and $\overline{\mathbf{24}}$ is a *Z*/*E*-isomeric relationship (a kind of 'diastereomeric' relationship) at the same time. This type of degeneration is well-known under the name of 'geometric enantiomers' (cf. page 85 of [49] and page 8 of [50]). Strictly speaking, the degeneration is not explicitly represented by Eq. 64. The last part of Eq. 64 should be modified as follows:

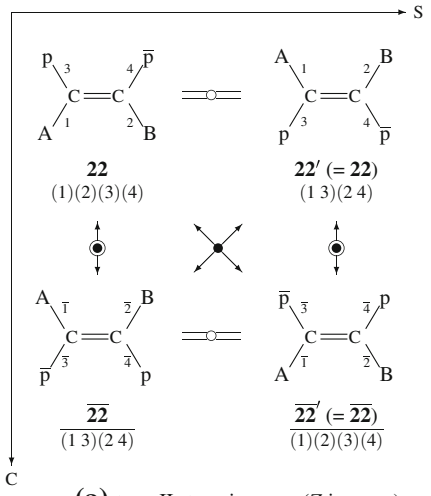

(a) type-II stereoisogram (*Z*-isomers)

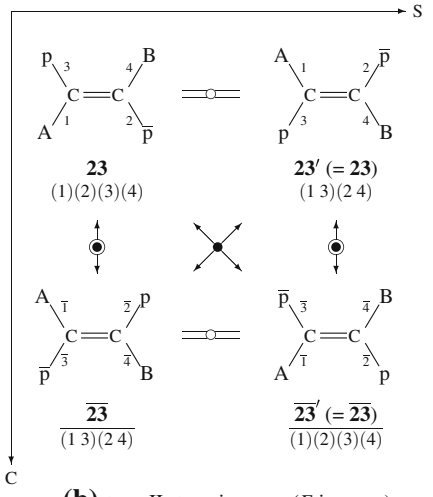

(b) type-II stereoisogram (*E*-isomers)

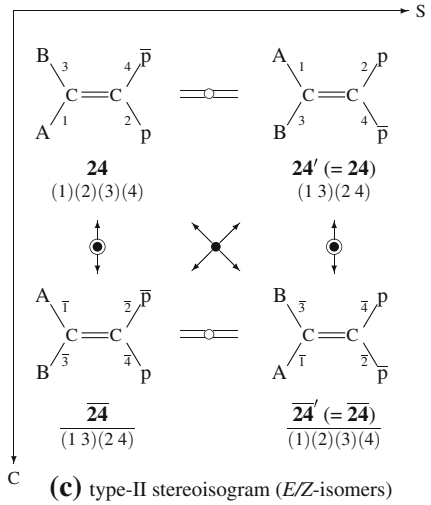

(c) type-II stereoisogram (*E/Z*-isomers)

Fig. 8 Stereoisograms for the composition ABp$\overline{\text{p}}$ on the basis of the ethylene skeleton. **a** A type-II stereoisogram containing a pair of enantiomers (*Z*-isomers). **b** A type-II stereoisogram containing a pair of enantiomers (*E*-isomers). **c** A type-II stereoisogram containing a pair of enantiomers (*E/Z*-isomers)

$$\left\langle \left(\left[\begin{matrix} \mathbf{24} \\ \overline{\mathbf{24}} \end{matrix} \right] \right) \left(\left[\begin{matrix} \overline{\mathbf{24}} \\ \mathbf{24} \end{matrix} \right] \right) \right\rangle, \tag{65}$$

where the two pairs of parentheses represent the *Z/E*-isomeric relationship between **24** and $\overline{\mathbf{24}}$, while each pair of square brackets represents the enantiomeric relationship between **24** and $\overline{\mathbf{24}}$. See Fig. 14 of [35].

3.4 Oxirane skeleton

The oxirane skeleton **4** has the group hierarchy shown by Eq. 42, so that the CI-CF for $\mathbf{S}_{2\widehat{\sigma}}^{[4]}$ (Eq. 51) is used to calculate the numbers of pairs of (self-)enantiomers under the point group $\mathbf{C}_{2v}$. The calculated values are collected in the PG-column of Table 5. The *RS*-SIG-column of Table 5 has been calculated by using the CI-CF for $\mathbf{S}_{6\widehat{I}}^{[4]}$ (Eq. 49), because the *RS*-stereoisomeric group $\mathbf{C}_{2v\widetilde{\sigma}\widehat{I}}$ for he oxirane skeleton **4** is isomorphic to $\mathbf{S}_{6\widehat{I}}^{[4]}$. The SIG-column of Table 5 (for the stereoisomeric group) has been obtained

Table 5 Numbers of isomers derived from an oxirane skeleton

Partition	PG $\mathbf{S}_{2\widehat{\sigma}}^{[4]}$ ($\mathbf{C}_{2v}$)	*RS*-SIG $\mathbf{S}_{6\widehat{I}}^{[4]}$ ($\mathbf{C}_{2v\widetilde{\sigma}\widehat{I}}$)	SIG $\mathbf{S}_{9\sigma\widehat{I}}^{[4]}$	ISG $\mathbf{S}_{\sigma\widehat{I}}^{[4]}$
$[\theta]_1 = [4,0,0,0;0,0,0,0,0,0,0,0,0]$	1	1	1	1
$[\theta]_2 = [3,1,0,0;0,0,0,0,0,0,0,0,0]$	1	1	1	1
$[\theta]_3 = [3,0,0,0;1,0,0,0,0,0,0,0,0]$	1	1/2	1/2	1/2
$[\theta]_4 = [2,2,0,0;0,0,0,0,0,0,0,0,0]$	3	3	2	1
$[\theta]_5 = [2,0,0,0;2,0,0,0,0,0,0,0,0]$	2	3/2	1	1/2
$[\theta]_6 = [2,1,1,0;0,0,0,0,0,0,0,0,0]$	3	3	2	1
$[\theta]_7 = [2,1,0,0;1,0,0,0,0,0,0,0,0]$	3	3/2	1	1/2
$[\theta]_8 = [2,0,0,0;1,1,0,0,0,0,0,0,0]$	5	3	2	1
$[\theta]_9 = [2,0,0,0;1,0,1,0,0,0,0,0,0]$	3	3/2	1	1/2
$[\theta]_{10} = [1,1,1,1;0,0,0,0,0,0,0,0,0]$	6	6	3	1
$[\theta]_{11} = [1,1,1,0;1,0,0,0,0,0,0,0,0]$	6	3	3/2	1/2
$[\theta]_{12} = [1,1,0,0;2,0,0,0,0,0,0,0,0]$	3	3/2	1	1/2
$[\theta]_{13} = [1,1,0,0;1,1,0,0,0,0,0,0,0]$	6	3	2	1
$[\theta]_{14} = [1,1,0,0;1,0,1,0,0,0,0,0,0]$	6	3	3/2	1/2
$[\theta]_{15} = [1,0,0,0;3,0,0,0,0,0,0,0,0]$	1	1/2	1/2	1/2
$[\theta]_{16} = [1,0,0,0;2,1,0,0,0,0,0,0,0]$	3	3/2	1	1/2
$[\theta]_{17} = [1,0,0,0;2,0,1,0,0,0,0,0,0]$	3	3/2	1	1/2
$[\theta]_{18} = [1,0,0,0;1,1,1,0,0,0,0,0,0]$	6	3	3/2	1/2
$[\theta]_{19} = [1,0,0,0;1,0,1,0,1,0,0,0,0]$	6	3	3/2	1/2
$[\theta]_{20} = [0,0,0,0;4,0,0,0,0,0,0,0,0]$	1/2	1/2	1/2	1/2
$[\theta]_{21} = [0,0,0,0;3,1,0,0,0,0,0,0,0]$	1	1/2	1/2	1/2
$[\theta]_{22} = [0,0,0,0;3,0,1,0,0,0,0,0,0]$	1	1/2	1/2	1/2
$[\theta]_{23} = [0,0,0,0;2,2,0,0,0,0,0,0,0]$	4	3	2	1
$[\theta]_{24} = [0,0,0,0;2,1,1,0,0,0,0,0,0]$	3	3/2	1	1/2
$[\theta]_{25} = [0,0,0,0;2,0,2,0,0,0,0,0,0]$	2	3/2	1	1/2
$[\theta]_{26} = [0,0,0,0;2,0,1,1,0,0,0,0,0]$	3	3/2	1	1/2
$[\theta]_{27} = [0,0,0,0;2,0,1,0,1,0,0,0,0]$	3	3/2	1	1/2
$[\theta]_{28} = [0,0,0,0;1,1,1,1,0,0,0,0,0]$	10	6	3	1
$[\theta]_{29} = [0,0,0,0;1,1,1,0,1,0,0,0,0]$	6	3	3/2	1/2
$[\theta]_{30} = [0,0,0,0;1,0,1,0,1,0,1,0,0]$	6	3	3/2	1/2

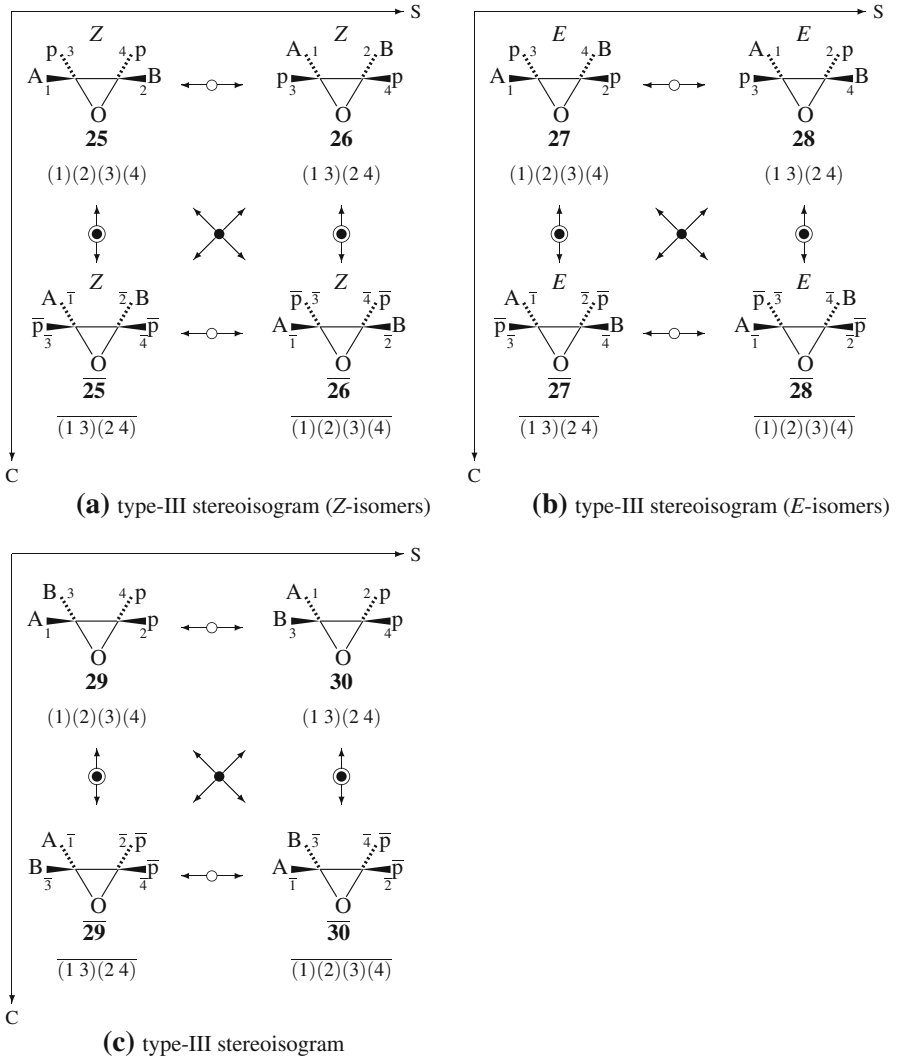

(a) type-III stereoisogram (*Z*-isomers)

(b) type-III stereoisogram (*E*-isomers)

(c) type-III stereoisogram

Fig. 9 Stereoisograms for the composition ABp^2 (or $AB\overline{p}^2$) on the basis of the oxirane skeleton. **a** A type-III stereoisogram containing two pairs of enantiomers (*Z*-isomers). **b** A type-III stereoisogram containing two pairs of enantiomers (*E*-isomers). **c** A type-III stereoisogram containing two pairs of enantiomers

by using the CI-CF for $\mathbf{S}^{[4]}_{9\sigma\widehat{I}}$ (Eq. 47) according to the group hierarchy (Eq. 42). The ISG-column of Table 5 (for the isoskeletal group) has been obtained by using the CI-CF for $\mathbf{S}^{[4]}_{\sigma\widehat{I}}$ (Eq. 45).

The value 3 at the intersection between $[\theta]_{12}$-row and the PG-column in Table 5 corresponds to $6 \times \frac{1}{2}(ABp^2 + AB\overline{p}^2)$, which indicates the appearance of six pairs of enantiomers. They are contained in the three type-III stereoisograms shown in Fig. 9. Thus, two pairs of enantiomers, **25**/$\overline{\mathbf{25}}$ and **26**/$\overline{\mathbf{26}}$, appear in the type-III stereoisogram shown in Fig. 9a; two pairs, **27**/$\overline{\mathbf{27}}$ and **28**/$\overline{\mathbf{28}}$, appear in the type-III stereoisogram

shown in Fig. 9b; and two pairs, **29**/$\overline{\mathbf{29}}$ and **30**/$\overline{\mathbf{30}}$, appear in the type-III stereoisogram shown in Fig. 9c.

The value 3/2 at the intersection between $[\theta]_{12}$-row and the *RS*-SIG-column in Table 5 corresponds to $3 \times \frac{1}{2}(\mathrm{ABp}^2 + \mathrm{AB}\overline{\mathrm{p}}^2)$, which indicates the appearance of three quadruplets of *RS*-stereoisomers, as confirmed by the three stereoisograms shown in Fig. 9.

In order to examine the the SIG-column, the *cis/trans*-isomerization of **25** (a *Z*-isomer) is confirmed to generate the corresponding *E*-isomer **27**. Hence, the stereoisogram shown by Fig. 9a is equivalent to the other stereoisogram shown by Fig. 9b under the action of the stereoisomeric group. Thereby, the quadruplets of the two stereoisograms coalesce into a single set of stereoisomers to be counted once for the SIG-column in Table 5.

On the other hand, the *cis/trans*-isomerization converts **29** into itself, so that the quadruplet of Fig. 9c itself generates a single set of stereoisomers to be counted once for the SIG-column in Table 5. Totally, there appear two inequivalent sets of stereoisomers, as found at the intersection between the $[\theta]_{12}$-row and the SIG-column in Table 5, where the value 1 corresponds to $2 \times \frac{1}{2}(\mathrm{ABp}^2 + \mathrm{AB}\overline{\mathrm{p}}^2)$.

Finally, the two inequivalent sets of stereoisomers (the value 1 at the SIG-column) are totally regarded as one set of isoskeletomers (the value 1/2 at the ISG-column). This result is also confirmed by Fig. 9, where the three stereoisograms coalesce to give a single set of isoskeletomers.

In summary, the hierarchy for the oxirane skeleton **4** (Eq. 42) results in the following classification for characterizing the $[\theta]_{12}$-row of Table 5:

$$\left\{\left\langle\left(\left[\frac{\mathbf{25}}{\mathbf{25}}\right]\left[\frac{\mathbf{26}}{\mathbf{26}}\right]\right)\left(\left[\frac{\mathbf{27}}{\mathbf{27}}\right]\left[\frac{\mathbf{28}}{\mathbf{28}}\right]\right)\right\rangle\left\langle\left(\left[\frac{\mathbf{29}}{\mathbf{29}}\right]\left[\frac{\mathbf{30}}{\mathbf{30}}\right]\right)\right\rangle\right\}, \tag{66}$$

where each pair of parentheses corresponds to each of the stereoisograms shown in Fig. 9. Remember that the number of pairs of square brackets indicates the number of inequivalent pairs of enantiomers, the number of pairs of parentheses indicates the number of inequivalent quadruplets of *RS*-stereoisomers, the number of pairs of angle brackets indicates the number of inequivalent sets of stereoisomers, and finally the number of pairs of braces indicates the number of inequivalent sets of isoskeletomers. The cases of the oxirane skeleton **4** exhibit non-degenerate features as exemplified by Eq. 66, where these numbers are at most different from one another in accord with the group hierarchy shown by Eq. 42.

The $[\theta]_{13}$-row of Table 5 corresponds to the composition $\mathrm{ABp}\overline{\mathrm{p}}$. The value 6 at the intersection between $[\theta]_{13}$-row and the PG-column in Table 5 indicates the presence of six pairs of enantiomers, as depicted in Fig. 10. The first type-III stereoisogram (Fig. 10a) consists of **31**/$\overline{\mathbf{31}}$ and **32**/$\overline{\mathbf{32}}$; the 2nd type-III stereoisogram (Fig. 10b) consists of **33**/$\overline{\mathbf{33}}$ and **34**/$\overline{\mathbf{34}}$; and the 3rd type-III stereoisogram (Fig. 10c) consists of **35**/$\overline{\mathbf{35}}$ and **36**/$\overline{\mathbf{36}}$.

The value 3 at the intersection between $[\theta]_{13}$-row and the *RS*-SIG-column in Table 5 indicates that there appear three quadruples of *RS*-stereoisomers, which construct the three stereoisograms shown in depicted in Fig. 10.

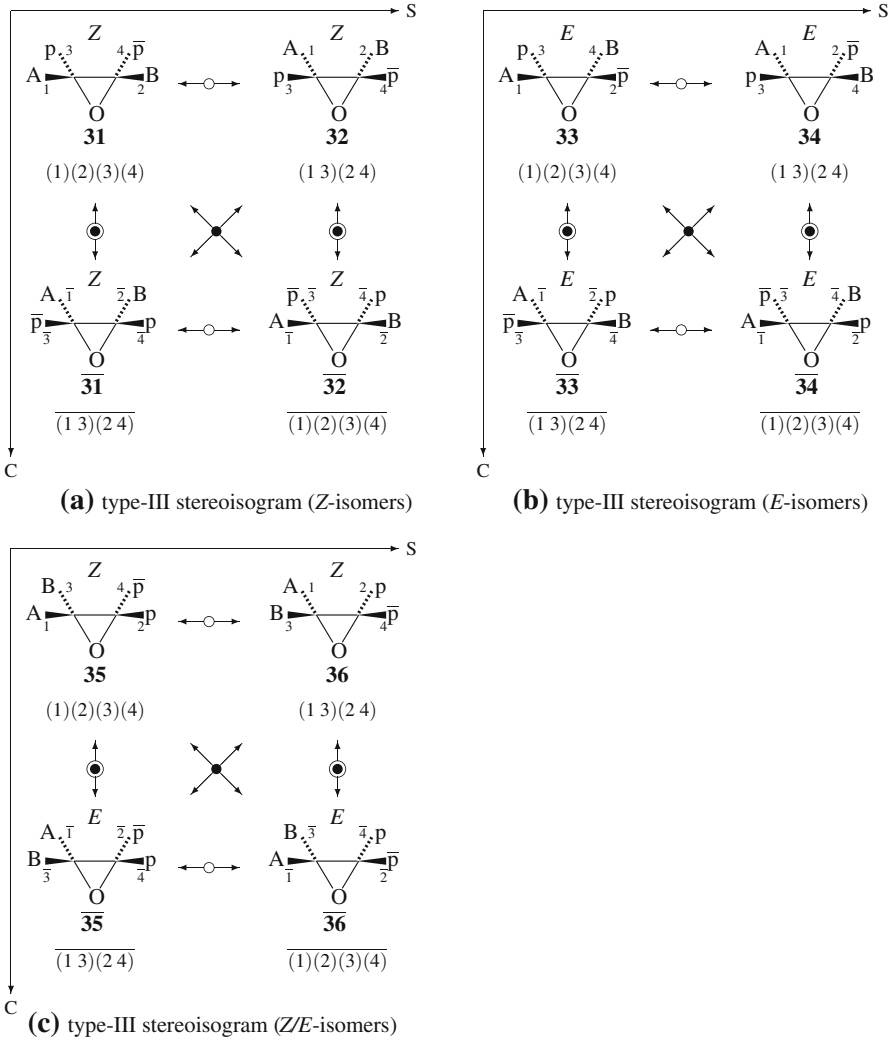

(a) type-III stereoisogram (*Z*-isomers)

(b) type-III stereoisogram (*E*-isomers)

(c) type-III stereoisogram (*Z*/*E*-isomers)

Fig. 10 Stereoisograms for the composition ABp$\overline{\text{p}}$ on the basis of the oxirane skeleton. **a** A type-III stereoisogram containing two pairs of enantiomers (*Z*-isomers). **b** A type-III stereoisogram containing two pairs of enantiomers (*E*-isomers). **c** A type-III stereoisogram containing two pairs of enantiomers (*Z*/*E*-isomers)

Because the *cis/trans*-isomerization of **31** (a *Z*-isomer) generates the corresponding *E*-isomer **33**, the stereoisogram shown by Fig. 10a is equivalent to the other stereoisogram shown by Fig. 10b under the action of the stereoisomeric group. Thereby, the quadruplets of the two stereoisograms coalesce into a single set of stereoisomers to be counted once for the SIG-column in Table 5. On the other hand, the *cis/trans*-isomerization converts **35** (a *Z*-isomer) into its enantiomer $\overline{\mathbf{35}}$ (an *E*-isomer), so that the quadruplet of Fig. 10c itself generates a single set of stereoisomers to be counted once for the SIG-column in Table 5. Totally, there appear two inequivalent sets of

stereoisomers in accord with the value 2 found at the intersection between the $[\theta]_{13}$-row and the SIG-column in Table 5.

Finally, the two inequivalent sets of stereoisomers (the value 2 at the SIG-column) are totally regarded as one set of isoskeletomers (the value 1 at the ISG-column). This result is also confirmed by Fig. 10, where the three stereoisograms coalesce to give a single set of isoskeletomers.

In summary, the hierarchy for the oxirane skeleton **4** (Eq. 42) results in the following classification for characterizing the $[\theta]_{13}$-row of Table 5:

$$\left\{\left\langle\left(\left[\frac{\mathbf{31}}{\mathbf{31}}\right]\left[\frac{\mathbf{32}}{\mathbf{32}}\right]\right)\left(\left[\frac{\mathbf{33}}{\mathbf{33}}\right]\left[\frac{\mathbf{34}}{\mathbf{34}}\right]\right)\right\rangle\left\langle\left(\left[\frac{\mathbf{35}}{\mathbf{35}}\right]\left[\frac{\mathbf{36}}{\mathbf{36}}\right]\right)\right\rangle\right\}, \tag{67}$$

where each pair of parentheses corresponds to each of the stereoisograms shown in Fig. 10.

It should be noted that the enantiomeric relationship between **35** and $\overline{\mathbf{35}}$ or between **36** and $\overline{\mathbf{36}}$ coalesce with a *Z*/*E*-isomeric relationship. See the interpretation described for Eq. 64.

3.5 Square planar skeleton

Because the square planar skeleton **5** has the group hierarchy shown by Eq. 43, the CI-CF for $\mathbf{S}^{[4]}_{9\sigma\widehat{I}}$ (Eq. 47) is used to calculate the numbers of pairs of enantiomers under the point group $\mathbf{D}_{4h}$. The calculated values are collected in the PG-column of Table 6. The *RS*-SIG-column of Table 6 is identical with the PG-column because of the group hierarchy shown by Eq. 43, where $\mathbf{S}^{[4]}_{9\sigma\widehat{I}}$ is isomorphic to the *RS*-stereoisomeric group $\mathbf{D}_{4\widehat{I}}$ for the square planar skeleton. The SIG-column of Table 6 (for the stereoisomeric group) has been obtained by using the CI-CF for $\mathbf{S}^{[4]}_{\sigma\widehat{I}}$ (Eq. 45) according to the group hierarchy (Eq. 43). The ISG-column of Table 6 (for the isoskeletal group) is identical with the SIG-column.

The $[\theta]_{13}$-row of Table 6 corresponds to the composition ABp$\overline{\text{p}}$. The value 2 at the intersection between $[\theta]_{13}$-row and the PG-column in Table 6 indicates the presence of two pairs of (self-)enantiomers. It follows that there emerge one pair of enantiomers **37**/$\overline{\mathbf{37}}$ and one achiral promolecule **38** (a pair of self-enantiomers), as depicted in Fig. 11.

The value 2 at the intersection between $[\theta]_{13}$-row and the *RS*-SIG-column in Table 6 is equal to that of the PG-column in accord with the group hierarchy shown by Eq. 43. The pair **37**/$\overline{\mathbf{37}}$ corresponds to the stereoisogram shown in Fig. 11a, while the achiral promolecule **38** corresponds to the stereoisogram shown in Fig. 11b. It follows that the two stereoisograms mean the presence of two quadruplets of *RS*-stereoisomers.

It should be noted that the stereoisograms shown in Fig. 11 are drawn by presuming the following coset decomposition:

$$\mathbf{D}_{4\widehat{I}} = \mathbf{C}_4 + \sigma\mathbf{C}_4 + \widetilde{\sigma}\mathbf{C}_4 + \widehat{I}\mathbf{C}_4, \tag{68}$$

which is derived from $\mathbf{D}_4 = \mathbf{C}_4 + \widetilde{\sigma}\mathbf{C}_4$.

Table 6 Numbers of isomers derived from a square planar skeleton

Partition	PG $\mathbf{S}^{[4]}_{9\sigma\widehat{I}}$ ($\mathbf{D}_{4h}$)	*RS*-SIG $\mathbf{S}^{[4]}_{9\sigma\widehat{I}}$ ($\mathbf{D}_{4\widehat{I}}$)	SIG $\mathbf{S}^{[4]}_{\sigma\widehat{I}}$	ISG $\mathbf{S}^{[4]}_{\sigma\widehat{I}}$
$[\theta]_1 = [4, 0, 0, 0; 0, 0, 0, 0, 0, 0, 0, 0]$	1	1	1	1
$[\theta]_2 = [3, 1, 0, 0; 0, 0, 0, 0, 0, 0, 0, 0]$	1	1	1	1
$[\theta]_3 = [3, 0, 0, 0; 1, 0, 0, 0, 0, 0, 0, 0]$	1/2	1/2	1/2	1/2
$[\theta]_4 = [2, 2, 0, 0; 0, 0, 0, 0, 0, 0, 0, 0]$	2	2	1	1
$[\theta]_5 = [2, 0, 0, 0; 2, 0, 0, 0, 0, 0, 0, 0]$	1	1	1/2	1/2
$[\theta]_6 = [2, 1, 1, 0; 0, 0, 0, 0, 0, 0, 0, 0]$	2	2	1	1
$[\theta]_7 = [2, 1, 0, 0; 1, 0, 0, 0, 0, 0, 0, 0]$	1	1	1/2	1/2
$[\theta]_8 = [2, 0, 0, 0; 1, 1, 0, 0, 0, 0, 0, 0]$	2	2	1	1
$[\theta]_9 = [2, 0, 0, 0; 1, 0, 1, 0, 0, 0, 0, 0]$	1	1	1/2	1/2
$[\theta]_{10} = [1, 1, 1, 1; 0, 0, 0, 0, 0, 0, 0, 0]$	3	3	1	1
$[\theta]_{11} = [1, 1, 1, 0; 1, 0, 0, 0, 0, 0, 0, 0]$	3/2	3/2	1/2	1/2
$[\theta]_{12} = [1, 1, 0, 0; 2, 0, 0, 0, 0, 0, 0, 0]$	1	1	1/2	1/2
$[\theta]_{13} = [1, 1, 0, 0; 1, 1, 0, 0, 0, 0, 0, 0]$	2	2	1	1
$[\theta]_{14} = [1, 1, 0, 0; 1, 0, 1, 0, 0, 0, 0, 0]$	3/2	3/2	1/2	1/2
$[\theta]_{15} = [1, 0, 0, 0; 3, 0, 0, 0, 0, 0, 0, 0]$	1/2	1/2	1/2	1/2
$[\theta]_{16} = [1, 0, 0, 0; 2, 1, 0, 0, 0, 0, 0, 0]$	1	1	1/2	1/2
$[\theta]_{17} = [1, 0, 0, 0; 2, 0, 1, 0, 0, 0, 0, 0]$	1	1	1/2	1/2
$[\theta]_{18} = [1, 0, 0, 0; 1, 1, 1, 0, 0, 0, 0, 0]$	3/2	3/2	1/2	1/2
$[\theta]_{19} = [1, 0, 0, 0; 1, 0, 1, 0, 1, 0, 0, 0]$	3/2	3/2	1/2	1/2
$[\theta]_{20} = [0, 0, 0, 0; 4, 0, 0, 0, 0, 0, 0, 0]$	1/2	1/2	1/2	1/2
$[\theta]_{21} = [0, 0, 0, 0; 3, 1, 0, 0, 0, 0, 0, 0]$	1/2	1/2	1/2	1/2
$[\theta]_{22} = [0, 0, 0, 0; 3, 0, 1, 0, 0, 0, 0, 0]$	1/2	1/2	1/2	1/2
$[\theta]_{23} = [0, 0, 0, 0; 2, 2, 0, 0, 0, 0, 0, 0]$	2	2	1	1
$[\theta]_{24} = [0, 0, 0, 0; 2, 1, 1, 0, 0, 0, 0, 0]$	1	1	1/2	1/2
$[\theta]_{25} = [0, 0, 0, 0; 2, 0, 2, 0, 0, 0, 0, 0]$	1	1	1/2	1/2
$[\theta]_{26} = [0, 0, 0, 0; 2, 0, 1, 1, 0, 0, 0, 0]$	1	1	1/2	1/2
$[\theta]_{27} = [0, 0, 0, 0; 2, 0, 1, 0, 1, 0, 0, 0]$	1	1	1/2	1/2
$[\theta]_{28} = [0, 0, 0, 0; 1, 1, 1, 1, 0, 0, 0, 0]$	3	3	1	1
$[\theta]_{29} = [0, 0, 0, 0; 1, 1, 1, 0, 1, 0, 0, 0]$	3/2	3/2	1/2	1/2
$[\theta]_{30} = [0, 0, 0, 0; 1, 0, 1, 0, 1, 0, 1, 0]$	3/2	3/2	1/2	1/2

The value 1 at the intersection between $[\theta]_{13}$-row and the SIG-column in Table 6 means that two quadruplets of Fig. 11 coalesce into a set of stereoisomers, which is counted once under the stereoisomeric group. The value of the ISG-column is identical with that of the SIG-column in accord with the group hierarchy shown by Eq. 43. This result of combinatorial enumeration is consistent with the extended stereoisogram denoted by II=II-IV which has been obtained by manual enumeration (e.g., Fig. 9 of [36]).

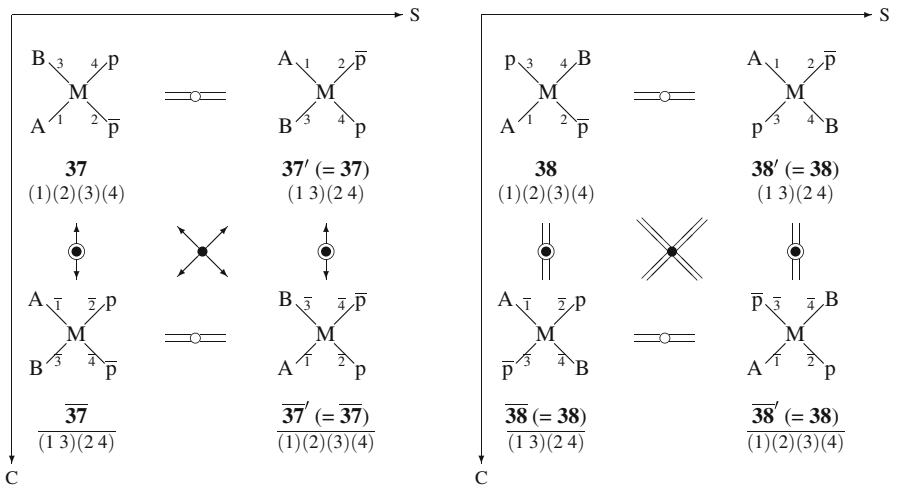

(a) type-II stereoisogram (*SP*-4-3,*SP*-4-4) **(b)** type-IV stereoisogram (*SP*-4-2)

Fig. 11 Stereoisograms for the composition ABp$\overline{\text{p}}$ on the basis of the square planar skeleton. **a** A type-II stereoisogram containing one pair of enantiomers (*SP*-4-3, *SP*-4-4). **b** A type-IV stereoisogram containing an achiral promolecule (*SP*-4-2)

In summary, the hierarchy for the square planar skeleton **5** (Eq. 43) results in the following classification for characterizing the $[\theta]_{13}$-row of Table 6:

$$\left\{\left\langle\left([\mathbf{37}\ \overline{\mathbf{37}}]\right)\left([\mathbf{38}]\right)\right\rangle\right\}, \tag{69}$$

where a pair of square brackets represents a pair of enantiomers as two-membered equivalence class or an achiral promolecule as one-membered equivalence class under the point group.

It should be noted that the enantiomeric relationship between **37** and $\overline{\mathbf{37}}$ coalesces with a 'diastereomeric' relationship (*SP*-4-3 versus *SP*-4-4), as shown in Fig. 11a. See the interpretation described for Eq. 64.

3.6 Square pyramidal skeleton

The square pyramidal skeleton **6** is characterized by the group hierarchy of Eq. 44. Hence, the CI-CF for $\mathbf{S}^{[4]}_{5\sigma\widehat{\sigma}}$ (Eq. 50) is used to calculate the numbers of pairs of (self-)enantiomers under the point group $\mathbf{C}_{4v}$. The calculated values are collected in the PG-column of Table 7. The *RS*-SIG-column of Table 7 is calculated by using the CI-CF for $\mathbf{S}^{[4]}_{9\sigma\widehat{I}}$ (Eq. 47), because $\mathbf{S}^{[4]}_{9\sigma\widehat{I}}$ is isomorphic to the *RS*-stereoisomeric group $\mathbf{C}_{4v\widetilde{\sigma}\widehat{I}}$ for the square pyramidal skeleton. The SIG-column of Table 7 (for the stereoisomeric group) has been obtained by using the CI-CF for $\mathbf{S}^{[4]}_{\sigma\widehat{I}}$ (Eq. 45) according to the group hierarchy (Eq. 43). The ISG-column of Table 6 (for the isoskeletal group) is identical with the SIG-column.

The $[\theta]_{13}$-row of Table 7 corresponds to the composition ABp$\overline{\text{p}}$. The value 4 at the intersection between the $[\theta]_{13}$-row and the PG-column in Table 7 indicates the

Table 7 Numbers of isomers derived from a square pyramidal skeleton

Partition	PG $\mathbf{S}^{[4]}_{5\sigma\widehat{\sigma}}$ ($\mathbf{C}_{4v}$)	*RS*-SIG $\mathbf{S}^{[4]}_{9\sigma\widehat{I}}$ ($\mathbf{C}_{4v\widetilde{\sigma}\widehat{I}}$)	SIG $\mathbf{S}^{[4]}_{\sigma\widehat{I}}$	ISG $\mathbf{S}^{[4]}_{\sigma\widehat{I}}$
$[\theta]_1 = [4, 0, 0, 0; 0, 0, 0, 0, 0, 0, 0, 0, 0]$	1	1	1	1
$[\theta]_2 = [3, 1, 0, 0; 0, 0, 0, 0, 0, 0, 0, 0, 0]$	1	1	1	1
$[\theta]_3 = [3, 0, 0, 0; 1, 0, 0, 0, 0, 0, 0, 0, 0]$	1/2	1/2	1/2	1/2
$[\theta]_4 = [2, 2, 0, 0; 0, 0, 0, 0, 0, 0, 0, 0, 0]$	2	2	1	1
$[\theta]_5 = [2, 0, 0, 0; 2, 0, 0, 0, 0, 0, 0, 0, 0]$	1	1	1/2	1/2
$[\theta]_6 = [2, 1, 1, 0; 0, 0, 0, 0, 0, 0, 0, 0, 0]$	2	2	1	1
$[\theta]_7 = [2, 1, 0, 0; 1, 0, 0, 0, 0, 0, 0, 0, 0]$	3/2	1	1/2	1/2
$[\theta]_8 = [2, 0, 0, 0; 1, 1, 0, 0, 0, 0, 0, 0, 0]$	3	2	1	1
$[\theta]_9 = [2, 0, 0, 0; 1, 0, 1, 0, 0, 0, 0, 0, 0]$	3/2	1	1/2	1/2
$[\theta]_{10} = [1, 1, 1, 1; 0, 0, 0, 0, 0, 0, 0, 0, 0]$	3	3	1	1
$[\theta]_{11} = [1, 1, 1, 0; 1, 0, 0, 0, 0, 0, 0, 0, 0]$	3	3/2	1/2	1/2
$[\theta]_{12} = [1, 1, 0, 0; 2, 0, 0, 0, 0, 0, 0, 0, 0]$	3/2	1	1/2	1/2
$[\theta]_{13} = [1, 1, 0, 0; 1, 1, 0, 0, 0, 0, 0, 0, 0]$	4	2	1	1
$[\theta]_{14} = [1, 1, 0, 0; 1, 0, 1, 0, 0, 0, 0, 0, 0]$	3	3/2	1/2	1/2
$[\theta]_{15} = [1, 0, 0, 0; 3, 0, 0, 0, 0, 0, 0, 0, 0]$	1/2	1/2	1/2	1/2
$[\theta]_{16} = [1, 0, 0, 0; 2, 1, 0, 0, 0, 0, 0, 0, 0]$	3/2	1	1/2	1/2
$[\theta]_{17} = [1, 0, 0, 0; 2, 0, 1, 0, 0, 0, 0, 0, 0]$	3/2	1	1/2	1/2
$[\theta]_{18} = [1, 0, 0, 0; 1, 1, 1, 0, 0, 0, 0, 0, 0]$	3	3/2	1/2	1/2
$[\theta]_{19} = [1, 0, 0, 0; 1, 0, 1, 0, 1, 0, 0, 0, 0]$	3	3/2	1/2	1/2
$[\theta]_{20} = [0, 0, 0, 0; 4, 0, 0, 0, 0, 0, 0, 0, 0]$	1/2	1/2	1/2	1/2
$[\theta]_{21} = [0, 0, 0, 0; 3, 1, 0, 0, 0, 0, 0, 0, 0]$	1/2	1/2	1/2	1/2
$[\theta]_{22} = [0, 0, 0, 0; 3, 0, 1, 0, 0, 0, 0, 0, 0]$	1/2	1/2	1/2	1/2
$[\theta]_{23} = [0, 0, 0, 0; 2, 2, 0, 0, 0, 0, 0, 0, 0]$	2	2	1	1
$[\theta]_{24} = [0, 0, 0, 0; 2, 1, 1, 0, 0, 0, 0, 0, 0]$	3/2	1	1/2	1/2
$[\theta]_{25} = [0, 0, 0, 0; 2, 0, 2, 0, 0, 0, 0, 0, 0]$	1	1	1/2	1/2
$[\theta]_{26} = [0, 0, 0, 0; 2, 0, 1, 1, 0, 0, 0, 0, 0]$	3/2	1	1/2	1/2
$[\theta]_{27} = [0, 0, 0, 0; 2, 0, 1, 0, 1, 0, 0, 0, 0]$	3/2	1	1/2	1/2
$[\theta]_{28} = [0, 0, 0, 0; 1, 1, 1, 1, 0, 0, 0, 0, 0]$	5	3	1	1
$[\theta]_{29} = [0, 0, 0, 0; 1, 1, 1, 0, 1, 0, 0, 0, 0]$	3	3/2	1/2	1/2
$[\theta]_{30} = [0, 0, 0, 0; 1, 0, 1, 0, 1, 0, 1, 0, 0]$	3	3/2	1/2	1/2

presence of four pairs of enantiomers, which are depicted in Fig. 12, i.e., **39**/$\overline{\mathbf{39}}$, **40**/$\overline{\mathbf{40}}$, **41**/$\overline{\mathbf{41}}$, and **42**/$\overline{\mathbf{42}}$.

The value 2 at the intersection between the $[\theta]_{13}$-row and the *RS*-SIG-column in Table 7 indicates that there appear two quadruplets of *RS*-stereoisomers under the action of the group $\mathbf{S}^{[4]}_{9\sigma\widehat{I}}$, which is isomorphic to $\mathbf{C}_{4v\widetilde{\sigma}\widehat{I}}$. Thus, the two pairs of enantiomers, **39**/$\overline{\mathbf{39}}$ and **40**/$\overline{\mathbf{40}}$, construct a quadruplet to be counted once, which is contained in a type III-stereoisogram (Fig. 12a). The other two pairs of enantiomers,

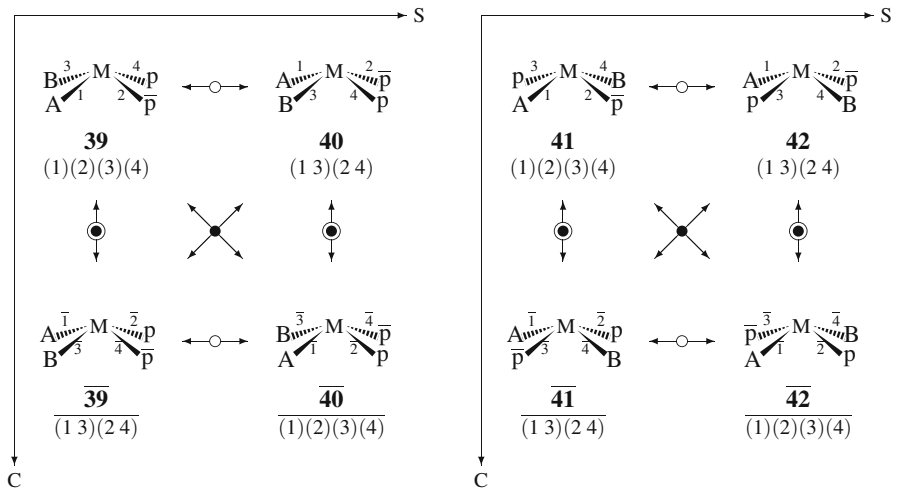

(a) type-III stereoisogram (*SPY*-4-3, *SPY*-4-4) **(b)** type-III stereoisogram (*SPY*-4-2)

Fig. 12 Stereoisograms for the composition ABp$\overline{\text{p}}$ on the basis of the square pyramidal skeleton. **a** A type-III stereoisogram containing two pairs of enantiomers (*SPY*-4-3, *SPY*-4-4). **b** A type-III stereoisogram containing two pairs of enantiomers (*SPY*-4-2)

41/$\overline{\textbf{41}}$ and **42**/$\overline{\textbf{42}}$, construct a quadruplet to be counted once, which is contained in another type III-stereoisogram (Fig. 12b).

The value 1 at the intersection between the $[\theta]_{13}$-row and the SIG-column in Table 7 means that two quadruplets of Fig. 12 coalesce into a set of stereoisomers, which is counted once under the stereoisomeric group. The value of the ISG-column is identical with that of the SIG-column in accord with the group hierarchy shown by Eq. 44.

In summary, the hierarchy for the square pyramidal skeleton **5** (Eq. 44) results in the following classification for characterizing the $[\theta]_{13}$-row of Table 6:

$$\{\langle([\mathbf{39}\ \overline{\mathbf{39}}]\ [\mathbf{40}\ \overline{\mathbf{40}}])\ ([\mathbf{41}\ \overline{\mathbf{41}}]\ [\mathbf{42}\ \overline{\mathbf{42}}])\rangle\}, \tag{70}$$

where a pair of square brackets represents a pair of enantiomers as two-membered equivalence class or an achiral promolecule as one-membered equivalence class under the point group.

It should be noted that the enantiomeric relationship between **39** and $\overline{\textbf{39}}$ (*C* versus *A*) or between **40** and $\overline{\textbf{40}}$ (*A* versus *C*) coalesces with a 'diastereomeric' relationship between **39** and $\overline{\textbf{39}}$ (*SPY*-4-3 versus *SPY*-4-4) or between **40** and $\overline{\textbf{40}}$ (*SPY*-4-3 versus *SPY*-4-4), as shown in Fig. 12a. See the interpretation described for Eq. 64.

4 Enumeration as graphs versus 3D structures

4.1 Modified Evaluation of Stereoisomers and Isoskeletomers

The enumerations in the preceding section adopt the compositions represented by the partitions $[\theta]_i$ ($i = 1$–30) in place of molecular formulas for counting isomers. It

follows that, for example, ABp^2 (counted by using $\frac{1}{2}(ABp^2 + AB\overline{p}^2)$ as a unit) and $ABp\overline{p}$ are counted separately, although they correspond to the same molecular formula. For the improved counting of inequivalent sets of stereoisomers (the SIG-column of each table) as well as inequivalent sets of isoskeletomers (the ISG-column of each table), the pair of proligands p/$\overline{p}$, q/$\overline{q}$, r/$\overline{r}$, or s/$\overline{s}$ should be considered to degenerate into a graph (2D structure), which is here denoted by the symbol $\ddot{p}$, $\ddot{q}$, $\ddot{r}$, or $\ddot{s}$.

To treat the stereoskeletons collected in Fig. 1 as graphs (2D structures), Eqs. 45 and 47 are converted to simplified cycle indices (CIs) without chirality fittingness, where the sphericity indices a_d, c_d, and b_d are replaced by a single dummy variable s_d.

$$\begin{aligned} \mathrm{CI}(\mathbf{S}^{[4]}_{\sigma\widehat{I}}) &= \frac{1}{48}\left(s_1^4 + 3s_2^2 + 8s_1s_3 + 6s_1^2s_2 + 6s_4 + 6s_1^2s_2 + 6s_4 + s_1^4 + 3s_2^2 + 8s_1a_3\right) \\ &= \frac{1}{24}\left(s_1^4 + 3s_2^2 + 8s_1s_3 + 6s_1^2s_2 + 6s_4\right) \end{aligned} \tag{71}$$

$$\begin{aligned} \mathrm{CI}(\mathbf{S}^{[4]}_{9\sigma\widehat{I}}) &= \frac{1}{16}\left(s_1^4 + 3s_2^2 + 2s_1^2b_2 + 2s_4 + 2s_1^2s_2 + 2s_4 + s_1^4 + 3s_2^2\right) \\ &= \frac{1}{8}\left(s_1^4 + 3s_2^2 + 2s_1^2b_2 + 2s_4\right) \end{aligned} \tag{72}$$

For the purpose of obtaining generating functions, Eqs. 53–55 are converted into a single ligand-inventory function:

$$s_d = \mathrm{A}^d + \mathrm{B}^d + \mathrm{X}^d + \mathrm{Y}^d + \ddot{\mathrm{p}}^d + \ddot{\mathrm{q}}^d + \ddot{\mathrm{r}}^d + \ddot{\mathrm{s}}^d, \tag{73}$$

where the symbol $\ddot{p}$, $\ddot{q}$, $\ddot{r}$, or $\ddot{s}$ appears with a coefficient 1 in accord with graph enumeration.

The ligand-inventory function (Eq. 73) is introduced into an CI (Eq. 71 or Eq. 72) to give a generating function, in which the coefficient of the term $\mathrm{A}^a\mathrm{B}^b\mathrm{X}^x\mathrm{Y}^y\ddot{\mathrm{p}}^{\ddot{p}}\ddot{\mathrm{q}}^{\ddot{q}}\ddot{\mathrm{r}}^{\ddot{r}}\ddot{\mathrm{s}}^{\ddot{s}}$ indicates the number of promolecules to be counted. Because the proligands A, B, etc. appear symmetrically, the term can be represented by the following partition:

$$[\ddot{\theta}] = [a, b, x, y;\ \ddot{p}, \ddot{q}, \ddot{r}, \ddot{s}], \tag{74}$$

where we put $a \geq b \geq x \geq y$ and $\ddot{p} \geq \ddot{q} \geq \ddot{r} \geq \ddot{s}$ without losing generality. For example, the partition $[\ddot{\theta}]_1 = [4, 0, 0, 0; 0, 0, 0, 0]$ corresponds to the terms A^4, B^4, and so on. The results are collected in the SIG′-column and the ISG′-column as found below.

On the other hand, the counting under the action of a point group (the PG-column) or an *RS*-stereoisomeric group (the *RS*-SIG-column) should be conducted by using one of the CI-CFs (Eqs. 45–51). To assure the consistency with the above graph enumeration, the ligand-inventory functions (Eqs. 53–55) are converted into the following equations:

$$a_d = \mathrm{A}^d + \mathrm{B}^d + \mathrm{X}^d + \mathrm{Y}^d \tag{75}$$

$$c_d = \mathrm{A}^d + \mathrm{B}^d + \mathrm{X}^d + \mathrm{Y}^d + 2\ddot{\mathrm{p}}^d + 2\ddot{\mathrm{q}}^d + 2\ddot{\mathrm{r}}^d + 2\ddot{\mathrm{s}}^d \tag{76}$$

$$b_d = \mathrm{A}^d + \mathrm{B}^d + \mathrm{X}^d + \mathrm{Y}^d + 2\ddot{\mathrm{p}}^d + 2\ddot{\mathrm{q}}^d + 2\ddot{\mathrm{r}}^d + 2\ddot{\mathrm{s}}^d, \tag{77}$$

where the symbol p̈, q̈, r̈, or s̈ appears with a coefficient 2 in accord with 3D structural enumeration. The results are collected in the PG′-column and the *RS*-SIG′-column as found below, where the partition represented by Eq. 74 is used.

4.2 Enumeration results and discussions

4.2.1 Tetrahedral skeleton

According to the group hierarchy shown by Eq. 39 for the tetrahedral skeleton **1**, the CI-CF for $\mathbf{S}_{10\sigma}^{[4]}$ (Eq. 46) is used to calculate the numbers of pairs of enantiomers under the point group $\mathbf{T}_d$, where the ligand-inventory functions Eqs. 75–77 are used in place of Eqs. 53–55. The resulting values are collected in the PG′-column of Table 8. On the other hand, the CI-CF for $\mathbf{S}_{\sigma\widehat{I}}^{[4]}$ (Eq. 45) and the ligand-inventory functions represented by Eqs. 75–77 are used to calculate the numbers of quadruplets of *RS*-stereoisomers under the *RS*-stereoisomeric group $\mathbf{T}_{d\widetilde{\sigma}\widehat{I}}$. The results are collected in the *RS*-SIG′-column of Table 8.

The numbers of inequivalent sets of stereoisomers are calculated by using the CI (Eq. 71) of the stereoisomeric group $\mathbf{S}_{\sigma\widehat{I}}^{[4]}$ and the ligand-inventory function represented by Eq. 73. The results are collected in the SIG′-column of Table 8. The ISG′-column

Table 8 Numbers of isomers derived from a tetrahedral skeleton

Partition	PG′ $\mathbf{S}_{10\sigma}^{[4]}$ ($\mathbf{T}_d$)	*RS*-SIG′ $\mathbf{S}_{\sigma\widehat{I}}^{[4]}$ ($\mathbf{T}_{d\widetilde{\sigma}\widehat{I}}$)	SIG′ $\mathbf{S}_{\sigma\widehat{I}}^{[4]}$	ISG′ $\mathbf{S}_{\sigma\widehat{I}}^{[4]}$
$[\ddot{\theta}]_1 = [4,0,0,0;0,0,0,0]$	1	1	1	1
$[\ddot{\theta}]_2 = [3,1,0,0;0,0,0,0]$	1	1	1	1
$[\ddot{\theta}]_3 = [3,0,0,0;1,0,0,0]$	1	1	1	1
$[\ddot{\theta}]_4 = [2,2,0,0;0,0,0,0]$	1	1	1	1
$[\ddot{\theta}]_5 = [2,0,0,0;2,0,0,0]$	2	2	1	1
$[\ddot{\theta}]_6 = [2,1,1,0;0,0,0,0]$	1	1	1	1
$[\ddot{\theta}]_7 = [2,1,0,0;1,0,0,0]$	1	1	1	1
$[\ddot{\theta}]_8 = [2,0,0,0;1,1,0,0]$	2	2	1	1
$[\ddot{\theta}]_9 = [1,1,1,1;0,0,0,0]$	1	1	1	1
$[\ddot{\theta}]_{10} = [1,1,1,0;1,0,0,0]$	2	1	1	1
$[\ddot{\theta}]_{11} = [1,1,0,0;2,0,0,0]$	3	2	1	1
$[\ddot{\theta}]_{12} = [1,1,0,0;1,1,0,0]$	4	2	1	1
$[\ddot{\theta}]_{13} = [1,0,0,0;3,0,0,0]$	2	2	1	1
$[\ddot{\theta}]_{14} = [1,0,0,0;2,1,0,0]$	4	3	1	1
$[\ddot{\theta}]_{15} = [1,0,0,0;1,1,1,0]$	8	4	1	1
$[\ddot{\theta}]_{16} = [0,0,0,0;4,0,0,0]$	3	3	1	1
$[\ddot{\theta}]_{17} = [0,0,0,0;3,1,0,0]$	4	4	1	1
$[\ddot{\theta}]_{18} = [0,0,0,0;2,2,0,0]$	5	5	1	1
$[\ddot{\theta}]_{19} = [0,0,0,0;2,1,1,0]$	8	6	1	1
$[\ddot{\theta}]_{20} = [0,0,0,0;1,1,1,1]$	16	8	1	1

Table 9 Correspondence of the two partitions

$[\ddot{\theta}]_1$	↔	$[\theta]_1$
$[\ddot{\theta}]_2$	↔	$[\theta]_2$
$[\ddot{\theta}]_3$	↔	$[\theta]_3$
$[\ddot{\theta}]_4$	↔	$[\theta]_4$
$[\ddot{\theta}]_5$	↔	$[\theta]_5$, $[\theta]_8$
$[\ddot{\theta}]_6$	↔	$[\theta]_6$
$[\ddot{\theta}]_7$	↔	$[\theta]_7$
$[\ddot{\theta}]_8$	↔	$[\theta]_9$ (2 times)
$[\ddot{\theta}]_9$	↔	$[\theta]_{10}$
$[\ddot{\theta}]_{10}$	↔	$[\theta]_{11}$
$[\ddot{\theta}]_{11}$	↔	$[\theta]_{12}$, $[\theta]_{13}$
$[\ddot{\theta}]_{12}$	↔	$[\theta]_{14}$ (2 times)
$[\ddot{\theta}]_{13}$	↔	$[\theta]_{15}$, $[\theta]_{16}$
$[\ddot{\theta}]_{14}$	↔	$[\theta]_{17}$ (2 times), $[\theta]_{18}$
$[\ddot{\theta}]_{15}$	↔	$[\theta]_{19}$ (4 times)
$[\ddot{\theta}]_{16}$	↔	$[\theta]_{20}$, $[\theta]_{21}$, $[\theta]_{23}$
$[\ddot{\theta}]_{17}$	↔	$[\theta]_{22}$ (2 times), $[\theta]_{24}$ (2 times)
$[\ddot{\theta}]_{18}$	↔	$[\theta]_{25}$ (2 times), $[\theta]_{26}$ (2 times), $[\theta]_{28}$
$[\ddot{\theta}]_{19}$	↔	$[\theta]_{27}$ (4 times), $[\theta]_{29}$ (2 times)
$[\ddot{\theta}]_{20}$	↔	$[\theta]_{30}$ (8 times)

(for the isoskeletal group) of Table 8 has equal values to those of the SIG′-column according to the group hierarchy (Eq. 39).

The comparison between Table 2 based on the compositions $[\theta]_i$ ($i = 1$–30) and Table 8 based on the compositions $[\ddot{\theta}]_j$ ($j = 1$–20) provides us with useful pieces of information on stereoisomerism. For the values in the PG′-column or in the *RS*-SIG′ (Table 8), the ligand inventory functions Eqs. 75–77 are used in place of Eqs. 53–55, although the same CI-CF ($\mathbf{S}^{[4]}_{10\sigma}$ or $\mathbf{S}^{[4]}_{\sigma\hat{I}}$) is used in comparison with the corresponding values in Table 2. Hence, the values based on the partitions $[\ddot{\theta}]_j$ ($j = 1$–20) in Table 8 are related to the values based on the partitions $[\theta]_i$ ($i = 1$–30) in Table 2, as collected in Table 9. For example, the value 16 at the intersection between $[\ddot{\theta}]_{20}$-row and PG′-column in Table 8 is correlated to the value 1 (corresponding to $2 \times \frac{1}{2}(\mathrm{pqrs} + \overline{\mathrm{pqrs}})$) at the intersection between $[\theta]_{30}$-row and the PG-column in Table 8), because the term $8 \times 2 \times \frac{1}{2}(\mathrm{pqrs} + \overline{\mathrm{pqrs}})$ corresponds to the term $8 \times 2 \times \ddot{\mathrm{p}}\ddot{\mathrm{q}}\ddot{\mathrm{r}}\ddot{\mathrm{s}}$. Note that the partition $[\theta]_{30}$ represents eight compositions (pqrs, p$\bar{\mathrm{q}}$rs, and so on), which are summed up to give the partition $[\ddot{\theta}]_{20}$.

For the values in the SIG′-column or in the ISG′ (Table 8), the usage of the CI (Eq. 71) and the ligand-inventory function (Eq. 73) means that they are based on graphs (2D structures). For example, the value 1 at the intersection between the $[\ddot{\theta}]_{20}$-row and the SIG′-column in Table 8 indicates that the number of inequivalent sets of stereoisomers is calculated to be 1, which consists of 16 pairs of enantiomers, as found at the intersection between $[\ddot{\theta}]_{20}$-row and PG′-column.

The $[\ddot{\theta}]_{10}$-row of Table 8 corresponds to the $[\theta]_{11}$-row of Table 2. As found in the $[\ddot{\theta}]_{10}$-row of Table 9, the composition ABX$\ddot{\mathrm{p}}$ for Table 8 corresponds to the composition

$\frac{1}{2}$(ABXp + ABX$\overline{\text{p}}$) for Table 2. Hence, the classification represented by Eq. 57 holds true in this modified enumeration.

The $[\ddot{\theta}]_{11}$-row of Table 8 corresponds to the $[\theta]_{12}$-row and the $[\theta]_{13}$-row of Table 2, as found in the $[\ddot{\theta}]_{11}$-row of Table 9. The value 1/2 at the intersection between the $[\theta]_{12}$-row and the SIG-column in Table 2 ($1 \times \frac{1}{2}(\text{ABp}^2 + \text{AB}\overline{\text{p}}^2)$) and the value 1 at the intersection between the $[\theta]_{13}$-row and the SIG-column in Table 2 ($1 \times \text{ABp}\overline{\text{p}}$) are combined to give the value 1 at the intersection between the $[\ddot{\theta}]_{11}$-row and the SIG′-column in Table 8 ($1 \times \text{AB}\ddot{\text{p}}^2$).

Hence, the stereoisogram of Fig. 3 (for the composition $\frac{1}{2}(\text{ABp}^2 + \text{AB}\overline{\text{p}}^2)$) and the stereoisogram of Fig. 4 (for the composition ABp$\overline{\text{p}}$) are combined, so as to construct a set of stereoisomers (for the composition AB$\ddot{\text{p}}^2$). As a result, Eqs. 58 and 59 are combined to give the following classification for characterizing the $[\ddot{\theta}]_{11}$-row of Table 8:

$$\left\{\left\langle\left(\left[\frac{\mathbf{9}}{\mathbf{9}}\right]\right)([\mathbf{10}]\,[\mathbf{11}])\right\rangle\right\}. \tag{78}$$

Hence, Eq. 78 is in accord with the values appearing in the $[\ddot{\theta}]_{11}$-row of Table 8, where three pairs of square brackets indicate the number 3 of pairs of (self-)enantiomers (the PG′-column), two pairs of parentheses indicate the number 2 of quadruplets of *RS*-stereoisomers (the *RS*-SIG′-column), one pair of angle brackets indicates the number 1 of a set of stereoisomers (the SIG′-column), and one pair of braces indicates the number 1 of a set of isoskeletomers (the ISG′-column).

4.2.2 Allene skeleton

Because the group hierarchy for the allene skeleton **2** is given by Eq. 40, the CI-CF for $\mathbf{S}_{6\sigma}^{[4]}$ (Eq. 48) is used to calculate the numbers of pairs of enantiomers under the point group $\mathbf{D}_{2d}$, where the ligand-inventory functions Eqs. 75–77 are used in place of Eqs. 53–55. The calculated values are collected in the PG′-column of Table 10. On the other hand, the CI-CF for $\mathbf{S}_{9\sigma\widehat{I}}^{[4]}$ (Eq. 47) is used to calculate the numbers of quadruplets of *RS*-stereoisomers under the *RS*-stereoisomeric group $\mathbf{D}_{2d\widetilde{\sigma}\widehat{I}}$ on the basis of the ligand-inventory functions shown in Eqs. 75–77. The results are collected in the *RS*-SIG′-column of Table 10.

The numbers of inequivalent sets of stereoisomers are calculated by using the CI (Eq. 72) of the stereoisomeric group $\mathbf{S}_{9\sigma\widehat{I}}^{[4]}$ and the ligand-inventory function represented by Eq. 73. The results are collected in the SIG′-column of Table 10. Note that the CI-CF (Eq. 47) for the *RS*-SIG′-column and the CI (Eq. 72) for the SIG′-column are distinguished from each other, although these columns are based on the same group $\mathbf{S}_{9\sigma\widehat{I}}^{[4]}$. The ISG′-column (for the isoskeletal group) of Table 10 is obtained by using the CI (Eq. 71) according to the group hierarchy (Eq. 40).

The $[\ddot{\theta}]_{11}$-row of Table 10 corresponds to the $[\theta]_{12}$-row and the $[\theta]_{13}$-row of Table 3, as found in the $[\ddot{\theta}]_{11}$-row of Table 9.

The value 3/2 at the intersection between the $[\theta]_{12}$-row and the PG-column in Table 3 ($3 \times \frac{1}{2}(\text{ABp}^2 + \text{AB}\overline{\text{p}}^2)$) and the value 4 at the intersection between the $[\theta]_{13}$-row and the PG-column in Table 3 ($4 \times \text{ABp}\overline{\text{p}}$) are combined to give the value 7 (seven pairs

Table 10 Numbers of isomers derived from an allene skeleton

Partition	PG′ $\mathbf{S}_{6\sigma}^{[4]}$ ($\mathbf{D}_{2d}$)	*RS*-SIG′ $\mathbf{S}_{9\sigma\hat{I}}^{[4]}$ ($\mathbf{D}_{2d\tilde{\sigma}\hat{I}}$)	SIG′ $\mathbf{S}_{9\sigma\hat{I}}^{[4]}$	ISG′ $\mathbf{S}_{\sigma\hat{I}}^{[4]}$
$[\ddot{\theta}]_1 = [4,0,0,0;0,0,0,0]$	1	1	1	1
$[\ddot{\theta}]_2 = [3,1,0,0;0,0,0,0]$	1	1	1	1
$[\ddot{\theta}]_3 = [3,0,0,0;1,0,0,0]$	1	1	1	1
$[\ddot{\theta}]_4 = [2,2,0,0;0,0,0,0]$	2	2	2	1
$[\ddot{\theta}]_5 = [2,0,0,0;2,0,0,0]$	5	4	2	1
$[\ddot{\theta}]_6 = [2,1,1,0;0,0,0,0]$	2	2	2	1
$[\ddot{\theta}]_7 = [2,1,0,0;1,0,0,0]$	3	2	2	1
$[\ddot{\theta}]_8 = [2,0,0,0;1,1,0,0]$	6	4	2	1
$[\ddot{\theta}]_9 = [1,1,1,1;0,0,0,0]$	3	3	3	1
$[\ddot{\theta}]_{10} = [1,1,1,0;1,0,0,0]$	6	3	3	1
$[\ddot{\theta}]_{11} = [1,1,0,0;2,0,0,0]$	7	4	2	1
$[\ddot{\theta}]_{12} = [1,1,0,0;1,1,0,0]$	12	6	3	1
$[\ddot{\theta}]_{13} = [1,0,0,0;3,0,0,0]$	4	3	1	1
$[\ddot{\theta}]_{14} = [1,0,0,0;2,1,0,0]$	12	7	2	1
$[\ddot{\theta}]_{15} = [1,0,0,0;1,1,1,0]$	24	12	3	1
$[\ddot{\theta}]_{16} = [0,0,0,0;4,0,0,0]$	4	4	1	1
$[\ddot{\theta}]_{17} = [0,0,0,0;3,1,0,0]$	8	6	1	1
$[\ddot{\theta}]_{18} = [0,0,0,0;2,2,0,0]$	15	11	2	1
$[\ddot{\theta}]_{19} = [0,0,0,0;2,1,1,0]$	24	14	2	1
$[\ddot{\theta}]_{20} = [0,0,0,0;1,1,1,1]$	48	24	3	1

of (self-)enantiomers) at the intersection between the $[\ddot{\theta}]_{11}$-row and the PG′-column in Table 10 ($7 \times \mathrm{AB}\ddot{\mathrm{p}}^2$).

The value 1 at the intersection between the $[\theta]_{12}$-row and the *RS*-SIG-column in Table 3 ($2 \times \frac{1}{2}(\mathrm{ABp}^2 + \mathrm{AB}\overline{\mathrm{p}}^2)$) and the value 2 at the intersection between the $[\theta]_{13}$-row and the *RS*-SIG-column in Table 3 ($2 \times \mathrm{ABp}\overline{\mathrm{p}}$) are combined to give the value 4 (four quadruplets of *RS*-stereoisomers) at the intersection between the $[\ddot{\theta}]_{11}$-row and the *RS*-SIG′-column in Table 10 ($4 \times \mathrm{AB}\ddot{\mathrm{p}}^2$).

The value 1 at the intersection between the $[\theta]_{12}$-row and the SIG-column in Table 3 ($2 \times \frac{1}{2}(\mathrm{ABp}^2 + \mathrm{AB}\overline{\mathrm{p}}^2)$) and the value 2 at the intersection between the $[\theta]_{13}$-row and the SIG-column in Table 3 ($2 \times \mathrm{ABp}\overline{\mathrm{p}}$) are combined, so as to give the value 2 at the intersection between the $[\ddot{\theta}]_{11}$-row and the SIG′-column in Table 10 ($2 \times \mathrm{AB}\ddot{\mathrm{p}}^2$). To explain this degeneration, the type-II stereoisogram of Fig. 5a (for the composition $\frac{1}{2}(\mathrm{ABp}^2 + \mathrm{AB}\overline{\mathrm{p}}^2)$) and the type-V stereoisogram of Fig. 6a (for the composition $\mathrm{ABp}\overline{\mathrm{p}}$) are combined, so as to construct one set of stereoisomers (for the composition $\mathrm{AB}\ddot{\mathrm{p}}^2$). On the other hand, the type-III stereoisogram of Fig. 5b (for the composition $\frac{1}{2}(\mathrm{ABp}^2 + \mathrm{AB}\overline{\mathrm{p}}^2)$) and the type-III stereoisogram of Fig. 6b (for the composition $\mathrm{ABp}\overline{\mathrm{p}}$) are combined, so as to construct the other one set of stereoisomers (for the composition $\mathrm{AB}\ddot{\mathrm{p}}^2$). Hence, the value 2 at the intersection between the $[\ddot{\theta}]_{11}$-row and the SIG′-column in Table 10 ($2 \times \mathrm{AB}\ddot{\mathrm{p}}^2$) is confirmed by the appearance of the two inequivalent sets of stereoisomers.

As a result, Eqs. 60 and 61 are combined to give the following classification for characterizing the $[\ddot{\theta}]_{11}$-row of Table 10:

$$\left\{\left\langle\left(\left[\frac{\mathbf{12}}{\mathbf{12}}\right]\right)([\mathbf{15}]\,[\mathbf{16}])\right\rangle\left\langle\left(\left[\frac{\mathbf{13}}{\mathbf{13}}\right]\left[\frac{\mathbf{14}}{\mathbf{14}}\right]\right)\left(\left[\frac{\mathbf{17}}{\mathbf{17}}\right]\left[\frac{\mathbf{18}}{\mathbf{18}}\right]\right)\right\rangle\right\}. \tag{79}$$

Hence, Eq. 79 is consistent with the values appearing in the $[\ddot{\theta}]_{11}$-row of Table 10, where seven pairs of square brackets indicate the number 7 of pairs of (self-) enantiomers (the PG′-column), four pairs of parentheses indicate the number 4 of quadruplets of *RS*-stereoisomers (the *RS*-SIG′-column), two pairs of angle brackets indicate the number 2 of two sets of stereoisomers (the SIG′-column), and one pair of braces indicates the number 1 of a set of isoskeletomers (the ISG′-column).

4.2.3 Ethylene skeleton

The group hierarchy for the ethylene skeleton **3** is given by Eq. 41, so that the CI-CF for $\mathbf{S}_{6\widehat{I}}^{[4]}$ (Eq. 49) is used to calculate the numbers of pairs of enantiomers under the point group $\mathbf{D}_{2h}$, where the ligand-inventory functions Eqs. 75–77 are used in place of Eqs. 53–55. The calculated values are collected in the PG′-column of Table 11. The *RS*-SIG′-column of Table 11 is identical with the PG′-column of Table 11.

Table 11 Numbers of isomers derived from an ethylene skeleton

Partition	PG′ $\mathbf{S}_{6\widehat{I}}^{[4]}$ $(\mathbf{D}_{2h})$	*RS*-SIG′ $\mathbf{S}_{6\widehat{I}}^{[4]}$ $(\mathbf{D}_{2\widehat{I}})$	SIG′ $\mathbf{S}_{9\sigma\widehat{I}}^{[4]}$	ISG′ $\mathbf{S}_{\sigma\widehat{I}}^{[4]}$
$[\ddot{\theta}]_1 = [4,0,0,0;0,0,0,0]$	1	1	1	1
$[\ddot{\theta}]_2 = [3,1,0,0;0,0,0,0]$	1	1	1	1
$[\ddot{\theta}]_3 = [3,0,0,0;1,0,0,0]$	1	1	1	1
$[\ddot{\theta}]_4 = [2,2,0,0;0,0,0,0]$	3	3	2	1
$[\ddot{\theta}]_5 = [2,0,0,0;2,0,0,0]$	6	6	2	1
$[\ddot{\theta}]_6 = [2,1,1,0;0,0,0,0]$	3	3	2	1
$[\ddot{\theta}]_7 = [2,1,0,0;1,0,0,0]$	3	3	2	1
$[\ddot{\theta}]_8 = [2,0,0,0;1,1,0,0]$	6	6	2	1
$[\ddot{\theta}]_9 = [1,1,1,1;0,0,0,0]$	6	6	3	1
$[\ddot{\theta}]_{10} = [1,1,1,0;1,0,0,0]$	6	6	3	1
$[\ddot{\theta}]_{11} = [1,1,0,0;2,0,0,0]$	6	6	2	1
$[\ddot{\theta}]_{12} = [1,1,0,0;1,1,0,0]$	12	12	3	1
$[\ddot{\theta}]_{13} = [1,0,0,0;3,0,0,0]$	4	4	1	1
$[\ddot{\theta}]_{14} = [1,0,0,0;2,1,0,0]$	12	12	2	1
$[\ddot{\theta}]_{15} = [1,0,0,0;1,1,1,0]$	24	24	3	1
$[\ddot{\theta}]_{16} = [0,0,0,0;4,0,0,0]$	5	5	1	1
$[\ddot{\theta}]_{17} = [0,0,0,0;3,1,0,0]$	8	8	1	1
$[\ddot{\theta}]_{18} = [0,0,0,0;2,2,0,0]$	18	18	2	1
$[\ddot{\theta}]_{19} = [0,0,0,0;2,1,1,0]$	24	24	2	1
$[\ddot{\theta}]_{20} = [0,0,0,0;1,1,1,1]$	48	48	3	1

The numbers of inequivalent sets of stereoisomers are calculated by using the CI (Eq. 72) of the stereoisomeric group $\mathbf{S}^{[4]}_{9\sigma\widehat{I}}$ and the ligand-inventory function representing by Eq. 73. The results collected in the SIG′-column of Table 11 are identical with the the SIG′-column of Table 10 because the same group $\mathbf{S}^{[4]}_{9\sigma\widehat{I}}$ is applied to both of the columns. The ISG′-column (for the isoskeletal group) of Table 11 is obtained by using the CI (Eq. 71) according to the group hierarchy (Eq. 41).

The $[\ddot{\theta}]_{11}$-row of Table 11 corresponds to the $[\theta]_{12}$-row and the $[\theta]_{13}$-row of Table 4, as found in the $[\ddot{\theta}]_{11}$-row of Table 9. In a similar way to the $[\ddot{\theta}]_{11}$-row of Table 10 for the allene skeleton (cf. Eq. 79 derived from Eqs. 60 and 61), Eqs. 63 and 64 for the ethylene skeleton are combined to give the following classification for characterizing the $[\ddot{\theta}]_{11}$-row of Table 11:

$$\left\{\left\langle\left(\left[\frac{\mathbf{19}}{\mathbf{19}}\right]\right)\left(\left[\frac{\mathbf{20}}{\mathbf{20}}\right]\right)\left(\left[\frac{\mathbf{22}}{\mathbf{22}}\right]\right)\left(\left[\frac{\mathbf{23}}{\mathbf{23}}\right]\right)\right\rangle\left\langle\left(\left[\frac{\mathbf{21}}{\mathbf{21}}\right]\right)\left(\left[\frac{\mathbf{24}}{\mathbf{24}}\right]\right)\right\rangle\right\}. \tag{80}$$

Hence, Eq. 80 is consistent with the values appearing in the $[\ddot{\theta}]_{11}$-row of Table 11, where six pairs of square brackets indicate the number 6 of pairs of (self-)enantiomers (the PG′-column), six pairs of parentheses indicate the number 6 of quadruplets of *RS*-stereoisomers (the *RS*-SIG′-column), two pairs of angle brackets indicate the number 2 of two sets of stereoisomers (the SIG′-column), and one pair of braces indicates the number 1 of a set of isoskeletomers (the ISG′-column).

The validity of Eq. 80 can be confirmed diagrammatically. Thus, the two stereoisograms shown in Fig. 7a, b (for representing Z/E-isomers) and the two stereoisograms shown in Fig. 8a, b (for representing Z/E-isomers) are gathered to generate the one set of stereoisomers, which is enclosed in a pair of angle brackets in Eq. 80. On the other hand, the stereoisogram shown in Fig. 7c and the stereoisograms shown in Fig. 8c are gathered to generate the other one set of stereoisomers, which is enclosed in another pair of angle brackets in Eq. 80. Finally, the two sets of stereoisomers are equivalence under the action of the isoskeletal group $\mathbf{S}^{[4]}_{\sigma\widehat{I}}$, so that they are enclosed in a pair of braces in Eq. 80 and there appears the value 1 at the intersection between the $[\ddot{\theta}]_{11}$-row and the ISG′-column in Table 11.

4.2.4 Oxirane skeleton

Because the group hierarchy for the oxirane skeleton **4** is given by Eq. 42, the CI-CF for $\mathbf{S}^{[4]}_{2\widehat{\sigma}}$ (Eq. 51) is used to calculate the numbers of pairs of enantiomers under the point group $\mathbf{C}_{2v}$, where the ligand-inventory functions Eqs. 75–77 are used in place of Eqs. 53–55. The calculated values are collected in the PG′-column of Table 12. The *RS*-SIG′-column of Table 12 is calculated by using the CI-CF for $\mathbf{S}^{[4]}_{6\widehat{I}}$ (Eq. 49), where the ligand-inventory functions Eqs. 75–77 are used. The SIG′-column and the ISG′-column of Table 12 for the oxirane skeleton are identical with those of Table 11 for the ethylene skeleton because of the application of the same groups.

The $[\ddot{\theta}]_{11}$-row of Table 12 corresponds to the $[\theta]_{12}$-row and the $[\theta]_{13}$-row of Table 5, as found in the $[\ddot{\theta}]_{11}$-row of Table 9. In a similar way to the $[\ddot{\theta}]_{11}$-row of Table 10 for the allene skeleton (cf. Eq. 79 derived from Eqs. 60 and 61), Eqs. 66 and 67 for the

Table 12 Numbers of isomers derived from an oxirane skeleton

Partition	PG′ $\mathbf{S}_{2\widehat{\sigma}}^{[4]}$ ($\mathbf{C}_{2v}$)	*RS*-SIG′ $\mathbf{S}_{6\widehat{I}}^{[4]}$ ($\mathbf{C}_{2v\widetilde{\sigma}\widehat{I}}$)	SIG′ $\mathbf{S}_{9\sigma\widehat{I}}^{[4]}$	ISG′ $\mathbf{S}_{\sigma\widehat{I}}^{[4]}$
$[\ddot{\theta}]_1 = [4, 0, 0, 0; 0, 0, 0, 0]$	1	1	1	1
$[\ddot{\theta}]_2 = [3, 1, 0, 0; 0, 0, 0, 0]$	1	1	1	1
$[\ddot{\theta}]_3 = [3, 0, 0, 0; 1, 0, 0, 0]$	2	1	1	1
$[\ddot{\theta}]_4 = [2, 2, 0, 0; 0, 0, 0, 0]$	3	3	2	1
$[\ddot{\theta}]_5 = [2, 0, 0, 0; 2, 0, 0, 0]$	9	6	2	1
$[\ddot{\theta}]_6 = [2, 1, 1, 0; 0, 0, 0, 0]$	3	3	2	1
$[\ddot{\theta}]_7 = [2, 1, 0, 0; 1, 0, 0, 0]$	6	3	2	1
$[\ddot{\theta}]_8 = [2, 0, 0, 0; 1, 1, 0, 0]$	12	6	2	1
$[\ddot{\theta}]_9 = [1, 1, 1, 1; 0, 0, 0, 0]$	6	6	3	1
$[\ddot{\theta}]_{10} = [1, 1, 1, 0; 1, 0, 0, 0]$	12	6	3	1
$[\ddot{\theta}]_{11} = [1, 1, 0, 0; 2, 0, 0, 0]$	12	6	2	1
$[\ddot{\theta}]_{12} = [1, 1, 0, 0; 1, 1, 0, 0]$	24	12	3	1
$[\ddot{\theta}]_{13} = [1, 0, 0, 0; 3, 0, 0, 0]$	8	4	1	1
$[\ddot{\theta}]_{14} = [1, 0, 0, 0; 2, 1, 0, 0]$	24	12	2	1
$[\ddot{\theta}]_{15} = [1, 0, 0, 0; 1, 1, 1, 0]$	48	24	3	1
$[\ddot{\theta}]_{16} = [0, 0, 0, 0; 4, 0, 0, 0]$	7	5	1	1
$[\ddot{\theta}]_{17} = [0, 0, 0, 0; 3, 1, 0, 0]$	16	8	1	1
$[\ddot{\theta}]_{18} = [0, 0, 0, 0; 2, 2, 0, 0]$	30	18	2	1
$[\ddot{\theta}]_{19} = [0, 0, 0, 0; 2, 1, 1, 0]$	48	24	2	1
$[\ddot{\theta}]_{20} = [0, 0, 0, 0; 1, 1, 1, 1]$	96	48	3	1

oxirane skeleton are combined to give the following classification for characterizing the $[\ddot{\theta}]_{11}$-row of Table 12:

$$\left\{\left\langle\left(\left[\frac{\mathbf{25}}{\mathbf{25}}\right]\left[\frac{\mathbf{26}}{\mathbf{26}}\right]\right)\left(\left[\frac{\mathbf{27}}{\mathbf{27}}\right]\left[\frac{\mathbf{28}}{\mathbf{28}}\right]\right)\left(\left[\frac{\mathbf{31}}{\mathbf{31}}\right]\left[\frac{\mathbf{32}}{\mathbf{32}}\right]\right)\left(\left[\frac{\mathbf{33}}{\mathbf{33}}\right]\left[\frac{\mathbf{34}}{\mathbf{34}}\right]\right)\right\rangle \left\langle\left(\left[\frac{\mathbf{29}}{\mathbf{29}}\right]\left[\frac{\mathbf{30}}{\mathbf{30}}\right]\right)\left(\left[\frac{\mathbf{35}}{\mathbf{35}}\right]\left[\frac{\mathbf{36}}{\mathbf{36}}\right]\right)\right\rangle\right\}. \tag{81}$$

Hence, Eq. 81 is consistent with the values appearing in the $[\ddot{\theta}]_{11}$-row of Table 12, where twelve pairs of square brackets indicate the number 12 of pairs of (self-)enantiomers (the PG′-column), six pairs of parentheses indicate the number 6 of quadruplets of *RS*-stereoisomers (the *RS*-SIG′-column), two pairs of angle brackets indicate the number 2 of two sets of stereoisomers (the SIG′-column), and one pair of braces indicates the number 1 of a set of isoskeletomers (the ISG′-column).

By referring to the stereoisograms shown in Figs. 9 and 10, the validity of Eq. 81 can be confirmed diagrammatically. Thus, the two stereoisograms shown in Fig. 9a, b (for representing Z/E-isomers) and the two stereoisograms shown in Fig. 10a, b (for representing Z/E-isomers) are combined to generate the one set of stereoisomers, which is enclosed in a pair of angle brackets in Eq. 81. On the other hand, the stereoisogram

shown in Fig. 9c and the stereoisograms shown in Fig. 10c are combined to generate the other one set of stereoisomers, which is enclosed in another pair of angle brackets in Eq. 81. The two sets of stereoisomers are equivalent under the action of the isoskeletal group $\mathbf{S}^{[4]}_{\sigma\widehat{I}}$, They are enclosed in a pair of braces in Eq. 81, so that there appears the value 1 at the intersection between the $[\ddot{\theta}]_{11}$-row and the ISG′-column in Table 12.

4.2.5 Square planar skeleton

Because the group hierarchy for the square planar skeleton **5** is given by Eq. 43, the CI-CF for $\mathbf{S}^{[4]}_{9\sigma\widehat{I}}$ (Eq. 47) is used to calculate the numbers of pairs of enantiomers under the point group $\mathbf{D}_{4h}$, where the ligand-inventory functions Eqs. 75–77 are used in place of Eqs. 53–55. The calculated values are collected in the PG′-column of Table 13. The *RS*-SIG′-column of Table 13 is identical with the PG′-column. The SIG′-column and the ISG′-column of Table 13 for the square planar skeleton are identical with the ISG′-column of Table 11 for the ethylene skeleton because of the application of the same group.

According to the correspondence shown in Table 9, the $[\ddot{\theta}]_j$-row of Table 13 corresponds to the counterpart rows of Table 6.

Table 13 Numbers of isomers derived from a square planar skeleton

Partition	PG′ $\mathbf{S}^{[4]}_{9\sigma\widehat{I}}$ ($\mathbf{D}_{4h}$)	*RS*-SIG′ $\mathbf{S}^{[4]}_{9\sigma\widehat{I}}$ ($\mathbf{D}_{4\widehat{I}}$)	SIG′ $\mathbf{S}^{[4]}_{\sigma\widehat{I}}$	ISG′ $\mathbf{S}^{[4]}_{\sigma\widehat{I}}$
$[\ddot{\theta}]_1 = [4,0,0,0;0,0,0,0]$	1	1	1	1
$[\ddot{\theta}]_2 = [3,1,0,0;0,0,0,0]$	1	1	1	1
$[\ddot{\theta}]_3 = [3,0,0,0;1,0,0,0]$	1	1	1	1
$[\ddot{\theta}]_4 = [2,2,0,0;0,0,0,0]$	2	2	1	1
$[\ddot{\theta}]_5 = [2,0,0,0;2,0,0,0]$	4	4	1	1
$[\ddot{\theta}]_6 = [2,1,1,0;0,0,0,0]$	2	2	1	1
$[\ddot{\theta}]_7 = [2,1,0,0;1,0,0,0]$	2	2	1	1
$[\ddot{\theta}]_8 = [2,0,0,0;1,1,0,0]$	4	4	1	1
$[\ddot{\theta}]_9 = [1,1,1,1;0,0,0,0]$	3	3	1	1
$[\ddot{\theta}]_{10} = [1,1,1,0;1,0,0,0]$	3	3	1	1
$[\ddot{\theta}]_{11} = [1,1,0,0;2,0,0,0]$	4	4	1	1
$[\ddot{\theta}]_{12} = [1,1,0,0;1,1,0,0]$	6	6	1	1
$[\ddot{\theta}]_{13} = [1,0,0,0;3,0,0,0]$	3	3	1	1
$[\ddot{\theta}]_{14} = [1,0,0,0;2,1,0,0]$	7	7	1	1
$[\ddot{\theta}]_{15} = [1,0,0,0;1,1,1,0]$	12	12	1	1
$[\ddot{\theta}]_{16} = [0,0,0,0;4,0,0,0]$	4	4	1	1
$[\ddot{\theta}]_{17} = [0,0,0,0;3,1,0,0]$	6	6	1	1
$[\ddot{\theta}]_{18} = [0,0,0,0;2,2,0,0]$	11	11	1	1
$[\ddot{\theta}]_{19} = [0,0,0,0;2,1,1,0]$	14	14	1	1
$[\ddot{\theta}]_{20} = [0,0,0,0;1,1,1,1]$	24	24	1	1

For example, the $[\ddot{\theta}]_{11}$-row of Table 13 corresponds to the $[\theta]_{12}$-row and the $[\theta]_{13}$-row of Table 6. The value 1 at the intersection between the $[\theta]_{12}$-row and the PG-column in Table 6 ($2 \times \frac{1}{2}(\mathrm{ABp}^2 + \mathrm{AB}\overline{\mathrm{p}}^2)$) and the value 2 at the intersection between the $[\theta]_{13}$-row and the PG-column in Table 6 ($2 \times \mathrm{ABp}\overline{\mathrm{p}}$) are combined to give the value 4 (four pairs of (self-)enantiomers) at the intersection between the $[\ddot{\theta}]_{11}$-row and the PG′-column in Table 13 ($4 \times \mathrm{AB}\ddot{\mathrm{p}}^2$). The *RS*-SIG′-column in Table 13 is identical with the PG′-column.

The value 1/2 at the intersection between the $[\theta]_{12}$-row and the SIG-column in Table 6 ($1 \times \frac{1}{2}(\mathrm{ABp}^2 + \mathrm{AB}\overline{\mathrm{p}}^2)$) and the value 1 at the intersection between the $[\theta]_{13}$-row and the SIG-column in Table 6 ($1 \times \mathrm{ABp}\overline{\mathrm{p}}$) are combined to construct one set of stereoisomers. It follows that there appears the value 1 at the intersection between the $[\ddot{\theta}]_{11}$-row and the SIG′-column in Table 13 ($1 \times \mathrm{AB}\ddot{\mathrm{p}}^2$).

4.2.6 Square pyramidal skeleton

According to the group hierarchy for the square pyramidal skeleton **6** (Eq. 44), the CI-CF for $\mathbf{S}^{[4]}_{5\sigma\widehat{\sigma}}$ (Eq. 50) is used to calculate the numbers of pairs of enantiomers under the point group $\mathbf{C}_{4v}$, where Eqs. 75–77 are used as ligand-inventory functions. The calculated values are collected in the PG′-column of Table 14. The *RS*-SIG′-column of

Table 14 Numbers of isomers derived from a square pyramidal skeleton

Partition	PG′ $\mathbf{S}^{[4]}_{5\sigma\widehat{\sigma}}$ ($\mathbf{C}_{4v}$)	*RS*-SIG′ $\mathbf{S}^{[4]}_{9\sigma\widehat{I}}$ ($\mathbf{C}_{4v\widetilde{\sigma}\widehat{I}}$)	SIG′ $\mathbf{S}^{[4]}_{\sigma\widehat{I}}$	ISG′ $\mathbf{S}^{[4]}_{\sigma\widehat{I}}$
$[\ddot{\theta}]_1 = [4,0,0,0;0,0,0,0]$	1	1	1	1
$[\ddot{\theta}]_2 = [3,1,0,0;0,0,0,0]$	1	1	1	1
$[\ddot{\theta}]_3 = [3,0,0,0;1,0,0,0]$	1	1	1	1
$[\ddot{\theta}]_4 = [2,2,0,0;0,0,0,0]$	2	2	1	1
$[\ddot{\theta}]_5 = [2,0,0,0;2,0,0,0]$	5	4	1	1
$[\ddot{\theta}]_6 = [2,1,1,0;0,0,0,0]$	2	2	1	1
$[\ddot{\theta}]_7 = [2,1,0,0;1,0,0,0]$	3	2	1	1
$[\ddot{\theta}]_8 = [2,0,0,0;1,1,0,0]$	6	4	1	1
$[\ddot{\theta}]_9 = [1,1,1,1;0,0,0,0]$	3	3	1	1
$[\ddot{\theta}]_{10} = [1,1,1,0;1,0,0,0]$	6	3	1	1
$[\ddot{\theta}]_{11} = [1,1,0,0;2,0,0,0]$	7	4	1	1
$[\ddot{\theta}]_{12} = [1,1,0,0;1,1,0,0]$	12	6	1	1
$[\ddot{\theta}]_{13} = [1,0,0,0;3,0,0,0]$	4	3	1	1
$[\ddot{\theta}]_{14} = [1,0,0,0;2,1,0,0]$	12	7	1	1
$[\ddot{\theta}]_{15} = [1,0,0,0;1,1,1,0]$	24	12	1	1
$[\ddot{\theta}]_{16} = [0,0,0,0;4,0,0,0]$	4	4	1	1
$[\ddot{\theta}]_{17} = [0,0,0,0;3,1,0,0]$	8	6	1	1
$[\ddot{\theta}]_{18} = [0,0,0,0;2,2,0,0]$	15	11	1	1
$[\ddot{\theta}]_{19} = [0,0,0,0;2,1,1,0]$	24	14	1	1
$[\ddot{\theta}]_{20} = [0,0,0,0;1,1,1,1]$	48	24	1	1

Table 13 is calculated by using the CI-CF for $\mathbf{S}^{[4]}_{9\sigma\hat{I}}$ (Eq. 47), where the ligand-inventory functions Eqs. 75–77 are used. The SIG′-column and the ISG′-column of Table 14 for the square pyramidal skeleton are identical with the ISG′-column of Table 13 for the square planar skeleton because of the application of the same group.

The $[\ddot{\theta}]_j$-row of Table 14 corresponds to the counterpart rows of Table 7 according to the correspondence shown in Table 9.

For example, the $[\ddot{\theta}]_{11}$-row of Table 14 corresponds to the $[\theta]_{12}$-row and the $[\theta]_{13}$-row of Table 7. The value 3/2 at the intersection between the $[\theta]_{12}$-row and the PG-column in Table 7 ($3 \times \frac{1}{2}(\mathrm{ABp}^2 + \mathrm{AB}\overline{\mathrm{p}}^2)$) and the value 4 at the intersection between the $[\theta]_{13}$-row and the PG-column in Table 7 ($4 \times \mathrm{ABp}\overline{\mathrm{p}}$) are combined to give the value 7 (seven pairs of (self-)enantiomers) at the intersection between the $[\ddot{\theta}]_{11}$-row and the PG′-column in Table 14 ($7 \times \mathrm{AB}\ddot{\mathrm{p}}^2$). In a similar way, the *RS*-SIG′-column in Table 14 can be correlated to the counterparts in Table 7.

The value 1/2 at the intersection between the $[\theta]_{12}$-row and the SIG-column in Table 7 ($1 \times \frac{1}{2}(\mathrm{ABp}^2 + \mathrm{AB}\overline{\mathrm{p}}^2)$) and the value 1 at the intersection between the $[\theta]_{13}$-row and the SIG-column in Table 7 ($1 \times \mathrm{ABp}\overline{\mathrm{p}}$) are combined to construct one set of stereoisomers. It follows that there appears the value 1 at the intersection between the $[\ddot{\theta}]_{11}$-row and the SIG′-column in Table 14 ($1 \times \mathrm{AB}\ddot{\mathrm{p}}^2$).

5 Conclusion

The proligand method developed originally for combinatorial enumeration under point groups [16–18] is extended to meet the group hierarchy due to the stereoisogram approach [29,30]. Thereby, it becomes applicable to enumeration under *RS*-stereoisomeric groups, under stereoisomeric groups, as well as under isoskeletal groups. Combinatorial enumerations are conducted to count pairs of (self-)enantiomers under a point group, quadruplets of *RS*-stereoisomers under an *RS*-stereoisomeric group, sets of stereoisomers under a stereoisomeric group, and sets of isoskeletomers under an isoskeletal group, where stereoskeletons of ligancy 4 (a tetrahedral skeleton, an allene skeleton, an ethylene skeleton, an oxirane skeleton, a square planar skeleton, and a square pyramidal skeleton) are used as examples. Two kinds of compositions are used for the purpose of representing molecular formulas in an abstract fashion, that is to say, the compositions represented by the partitions $[\theta]_i$ ($i = 1$–30) for differentiating proligands having opposite chirality senses and the compositions represented by the partitions $[\ddot{\theta}]_j$ ($i = 1$–20) for equalizing proligands having opposite chirality senses. Thereby, the classifications of isomers are accomplished in a systematic fashion.

References

1. G. Pólya, Acta Math. **68**, 145–254 (1937)
2. G. Pólya, R.C. Read, *Combinatorial Enumeration of Groups, Graphs, and Chemical Compounds* (Springer, New York, 1987)
3. F. Harary, in *Graph Theory and Theoretical Physics*, ed. by F. Harary (Academic Press, London, 1967), pp. 1–41
4. F. Harary, E.M. Palmer, R.W. Robinson, R.C. Read, in *Chemical Applications of Graph Theory*, ed. by A.T. Balaban (Academic, London, 1976), pp. 11–24

5. G.L. Liu, *Introduction to Combinatorial Mathematics* (McGraw Hill, New York, 1968)
6. F. Harary, Graph Theory (Addison-Wesley, Reading, 1969)
7. N.L. Biggs, E.K. Lloyd, R.J. Wilson, *Graph Theory 1736–1936* (Oxford University Press, Oxford, 1976)
8. F. Harary, E.M. Palmer, *Graphical Enumeration* (Academic Press, New York, 1973)
9. H. Hosoya, Kagaku no Ryoiki **26**, 989–1001 (1972)
10. D.H. Rouvray, Chem. Soc. Rev. **3**, 355–372 (1974)
11. O.E. Polansky, MATCH Commun. Math. Comput. Chem. **1**, 11–31 (1975)
12. K. Balasubramanian, Chem. Rev. **85**, 599–618 (1985)
13. A.T. Balaban (ed.), *Chemical Applications of Graph Theory* (Academic Press, London, 1976)
14. G. Pólya, R.E. Tarjan, D.R. Woods, *Notes on Introductory Combinatorics* (Birkhäuser, Boston, 1983)
15. N. Trinajstić, *Chemical Graph Theory*, vol. I and II (CRC Press, Boca Raton, 1983)
16. S. Fujita, Theor. Chem. Acc. **113**, 73–79 (2005)
17. S. Fujita, Theor. Chem. Acc. **113**, 80–86 (2005)
18. S. Fujita, Theor. Chem. Acc. **115**, 37–53 (2006)
19. S. Fujita, Croat. Chem. Acta **79**, 411–427 (2006)
20. S. Fujita, Theor. Chem. Acc. **117**, 353–370 (2007)
21. S. Fujita, Theor. Chem. Acc. **117**, 339–351 (2007)
22. S. Fujita, J. Math. Chem. **43**, 141–201 (2008)
23. S. Fujita, MATCH Commun. Math. Comput. Chem. **67**, 5–24 (2012)
24. S. Fujita, MATCH Commun. Math. Comput. Chem. **67**, 25–54 (2012)
25. S. Fujita, MATCH Commun. Math. Comput. Chem. **67**, 649–668 (2012)
26. S. Fujita, Bull. Chem. Soc. Jpn. **83**, 1–18 (2010)
27. S. Fujita, *Symmetry and Combinatorial Enumeration in Chemistry* (Springer, Berlin, 1991)
28. S. Fujita, *Combinatorial Enumeration of Graphs, Three-Dimensional Structures, and Chemical Compounds* (University of Kragujevac, Faculty of Science, Kragujevac, 2013)
29. S. Fujita, J. Org. Chem. **69**, 3158–3165 (2004)
30. S. Fujita, Tetrahedron **60**, 11629–11638 (2004)
31. S. Fujita, Tetrahedron: Asymmetry **23**, 623–634 (2012)
32. S. Fujita, J. Math. Chem. **50**, 2168–2201 (2012)
33. S. Fujita, J. Math. Chem. **35**, 265–287 (2004)
34. S. Fujita, MATCH Commun. Math. Comput. Chem. **52**, 3–18 (2004)
35. S. Fujita, J. Chem. Inf. Comput. Sci. **44**, 1719–1726 (2004)
36. S. Fujita, MATCH Commun. Math. Comput. Chem. **53**, 147–159 (2005)
37. S. Fujita, J. Am. Chem. Soc. **112**, 3390–3397 (1990)
38. S. Fujita, Tetrahedron **47**, 31–46 (1991)
39. S. Fujita, J. Math. Chem. **32**, 1–17 (2002)
40. S. Fujita, Bull. Chem. Soc. Jpn. **63**, 315–327 (1990)
41. S. Fujita, Helv. Chim. Acta **85**, 2440–2457 (2002)
42. S. Fujita, J. Math. Chem. **33**, 113–143 (2003)
43. S. Fujita, Polyhedron **12**, 95–110 (1993)
44. S. Fujita, J. Math. Chem. **52**, 508–542 (2014)
45. S. Fujita, MATCH Commun. Math. Comput. Chem. **54**, 39–52 (2005)
46. S. Fujita, J. Math. Chem. **52**, 1717–1750 (2014)
47. S. Fujita, J. Math. Chem. **52**, 1751–1793 (2014)
48. S. Fujita, Memoirs of the Faculty of Engineering and Design, vol. 53 (Kyoto Institute of Technology, 2005), pp. 19–38
49. K. Mislow, *Introduction to Stereochemistry* (Benjamin, New York, 1965)
50. G. Helmchen, A. General Aspects. 1. Nomenclature and vocabulary of organic stereochemistry, in *Stereoselective Synthesis. Methods of Organic Chemistry (Houben-Weyl)*. Workbench Edition E21, vol. 1, 4 edn., eds. by G. Helmchen, R.W. Hoffmann, J. Mulzer, E. Schaumann (Georg Thieme, Stuttgart, New York, 1996), pp. 1–74